Computational Modeling of Triple-Layered Microwave Heat Exchangers

by

Ajit Ashokrao Mohekar

A Thesis

Submitted to the Faculty

of the

WORCESTER POLYTECHNIC INSTITUTE

in partial fulfillment of the requirements for the

Degree of Master of Science

in

Mechanical Engineering

May 2018

APPROVED:

Professor Burt Tilley, Thesis Advisor	Professor Vadim Yakovlev, Thesis Co-advisor
Professor L. Ramdas Ram-Mohan, Committee Member	Professor Cosme Furlong-Vazquez, Graduate Committee Representative

Abstract

A microwave heat exchanger (MHE) is a device which converts microwave (MW) energy into usable form of heat energy. The working principle of the MHE is based on a collective effect of electromagnetic wave propagation, heat transfer and fluid flow, so the development of an efficient device requires complicated experimentation with processes of different physical nature. A peculiar phenomenon making the design of MHE even more challenging is *thermal runaway*, a nonlinear phenomenon in which a small increase in the input power gives rise to a large increase in temperature. Such high temperature may result in material damage through excessive thermal expansion, cracking, or melting. In this Thesis, we report on an initial phase in the development of a computational model which may help clarify complicated interaction between nonlinear phenomena that might be difficult to comprehend and control experimentally.

We present a 2D multiphysics model mimicking operation of a layered MHE that simulates the nonlinear interaction between MW, thermal, and fluid flow phenomena involved in the operation of the MHE. The model is built for a triple layered (fluid-ceramic-fluid) MHE and is capable of capturing the S- and SS-profiles of power response curve which determines steady-state temperature solution as a function of incident power.

The model is implemented on the platform of the COMSOL Multiphysics modeling software. We show that a MHE with particular thickness and dielectric properties of the layers can operate efficiently by keeping temperatures during thermal runaway under control. Overall temperatures increase rapidly as soon as the local maximum temperature reaches a critical value. This condition is held true both in absence and in presence of fluid flow. It is demonstrated that the efficiency of the MHE dramatically increases when thermal runaway is achieved. As the amount of heat energy, which is being transferred to the fluid from the heated dielectric, increases, incident power required to achieve thermal runaway also increases. It is also shown that, with appropriate length of the layered MHE,

thermal runaway can be achieved at a lower power level. While the model developed in this Thesis studies the basic operation of a three layered MHE, it can further be developed to investigate optimum design parameters of the MHE of other structures so that maximum thermal efficiency is achieved.

Significance of This Work

Traditionally microwave (MW) heating has been utilized in many applications such as processing of food products, microwave assisted chemistry, high temperature treatment of materials, etc. Relatively new devices are Microwave Heat Exchangers (MHE) which are used in solar thermal collectors, wireless energy transmissions, and microwave thermal thrusters. Future applications include beamed energy harnessing where a satellite is used to collect and convert solar energy into microwaves that will then be beamed to earth to help contribute to the energy production, and beamed energy propulsion where electromagnetic heating is utilized to create a thrust that can improve current rocket propulsion capabilities. A common thread in these technologies is the conversion of electromagnetic energy into a mechanically useful form.

Microwave heat exchnagers (MHE) allow conversion of MW energy into heat energy. In this work, we have developed the first numerical model of an efficient triple layered MHE. The model can help understand coupled interaction between multiple physical phenomena involved in the operation of a MHE. Further, the model can help engineers to decide on optimum design parameters so that maximum thermal efficiency is achieved.

Acknowledgment

I would first like to thank my thesis advisors Professor Burt Tilley and Professor Vadim Yakovlev of the Mathematical Science Department for their continuous support, guidance, and patience. When I started working with Professor Tilley and Professor Yakovlev, I never thought that I would be able to contribute to their research but their continuing faith in my work, encouraged me to push myself beyond my limits. I thank my fellow colleague, Joseph Gaone, Ph.D student at the Mathematical Science Department for helping me out in debugging my numerical model. Whenever I struggled with complicated concepts, Joe always explained everything very clearly. I also thank Dr. Brad Hoff of the AFRL, Kirtland AFB for his suggestions during my research.

I sincerely thank Professor Cosme Furlong-Vazquez of the Mechanical Engineering Department for being the second reader of this thesis, and I am indebted for his valuable comments on my Thesis. I also take this opportunity to thank Professor L. Ramdas Ram-Mohan of the Physics Department for being there as a committee member. Concepts I learned in his class have helped me understand complicated mathematics involved in modeling software packages. He has always been helpful whenever I encountered troubles.

I am grateful for the support from the Air Force Office of Scientific Research (AFOSR); Award: FA9550-15-0476. I would also like to thank the office of Academic and Research Computing at WPI for providing me access to high performance computers.

I must express my gratitude to my parents and my family for providing me with unfailing support and continuous encouragement throughout my years of study. This accomplishment would never have been possible without them.

Finally, I dedicate my thesis to both of my advisors, Professor Burt Tilley and Professor Vadim Yakovlev, and my parents. Thank you for everything!

Contents

List of Figures

List of Tables

List of Symbols

Q	Volumetric heat source generated due to microwave heating
σ	Electrical conductivity of the material
$\vec{E}$	Electric field
σ_{eff}	Effective electrical conductivity of the material
ϵ	Permittivity of the material
ϵ'	Real part of the permittivity
ϵ_0	Permittivity of the free space
ϵ'_r	Relative permittivity of the material
ϵ''	Imaginary part of the permittivity
μ	Permeability of the material
μ'	Real part of the permeability of the material
μ''	Imaginary part of the permeability of the material
μ'_r	Relative permeability of the medium
ρ	Density of the material
C_p	Specific heat capacity
T	Temperature
t	Time
$\vec{u}$	Velocity of the fluid
K	Thermal conductivity of the material
P	Pressure

ν	Kinematic viscosity of the fluid
$\vec{D}$	Electric flux density
$\vec{B}$	Magnetic flux density
ω	Angular velocity of the microwaves
c	Speed of electromagnetic waves in free space
k_0	Wavenumber of the free space
h	Heat transfer coefficient
ξ	Emissivity of the surface
T_A	Ambient temperature
σ_b	Stefan-Boltzmann Constant
P_{av}	Time average incident power density
E_0	Strength of the incident microwave
η	Characteristics impedance of the free space
l_1	Width of the fluid channel
l_2	Width of the lossy layer
λ	Wavelength of the microwave
S_j	Maximum size of the element
L	Length of the fluid channel

Chapter 1

Introduction

1.1 Background

A heat exchanger is a device used to transfer heat between a solid object and a fluid, or between two or more fluids (Frass in [1], Bergman et al. in [2], Kays in [3]). Household refrigerators, internal combustion engines used in cars, air conditioning systems, water heaters, etc., are some examples of popular heat exchnagers. Functional requirement of a heat exchanger depends on the application. An air conditioner efficiently extracts heat from the surrounding to provide cooling effect whereas a water heater supplies heat in order to heat the water. An electromagnetic heat exchanger converts electromagnetic (EM) energy into heat energy. Thus the functional requirement of an EM heat exchanger is to provide a mean of efficiently extracting heat energy from a material which is heated by EM waves.

Electromagnetic heating may occur due to two different sources (Metaxas in [4] and Willert-Porada in [5]). Eddy currents are generated in an electrically conducting material when in contact with alternating electric field. The eddy currents then flow through the resistance of the material, and heat it by Ohmic heating. Induction heaters are an example of such a heating. Microwave (MW) heating, also called as *dielectric heating*, occurs when an alternating electric field propagates through a material which contains polar molecules having an electric dipole moment. Since polar molecules have tendency to align themselves

with the electric field, they rotate rapidly when oscillating electric field penetrates in such a material. Temperature is a function of kinetic energy, and such rotation of dipoles increases average kinetic energy of molecules which in turn heats up the material. Heat generation during MW heating depends on the imaginary part of complex permittivity, also called as the loss factor, of the material. If the permittivity of a material is complex then the material is considered as a lossy material. When electric field propagates in a lossy material, its amplitude decays due to EM losses in the material. For some materials such as lossy ceramics, the imaginary part of the permittivity increases exponentially (Hill and Jennings in [6]) with temperature, which creates a positive feedback loop between complex permittivity and temperature. Such a positive feedback causes loss factor to increase even further as temperature increases, and thus might lead to a large temperature increase called as *thermal runaway*. Lossy ceramics that undergo thermal runaway can be either porous or containing fluid channels to accommodate continuously flowing coolant extracting heat from the lossy ceramic.

EM heat exchangers that operate in the range of microwave frequencies are called microwave heat exchangers (MHE). They are used in such applications such as solar thermal collector (Jamar et al. in [7]), wireless energy transmissions (Jawdat et al. in [8]), and microwave thermal thrusters (Parkin et al. in [9]), and others. Work is being done to use a satellite to collect and convert solar energy into MW that is then beamed to Earth in order to help contribute to energy production. From the other direction, energy generated on Earth could be transmitted to satellites to add to the power being generated by solar panels. In addition, beamed energy propulsion has also been proposed as a method of improving current rocket propulsion capabilities (Landis in [10], Coopersmith and Davis in [11]). One of the essential components in such applications is a MHE that can efficiently convert microwave energy into usable form of heat energy.

The working principle of MHE is governed by the nonlinear coupling between electromagnetic wave propagation, internal energy conservation, and fluid flow mass and momentum conservation, and thus require particularly extensive experimental developments.

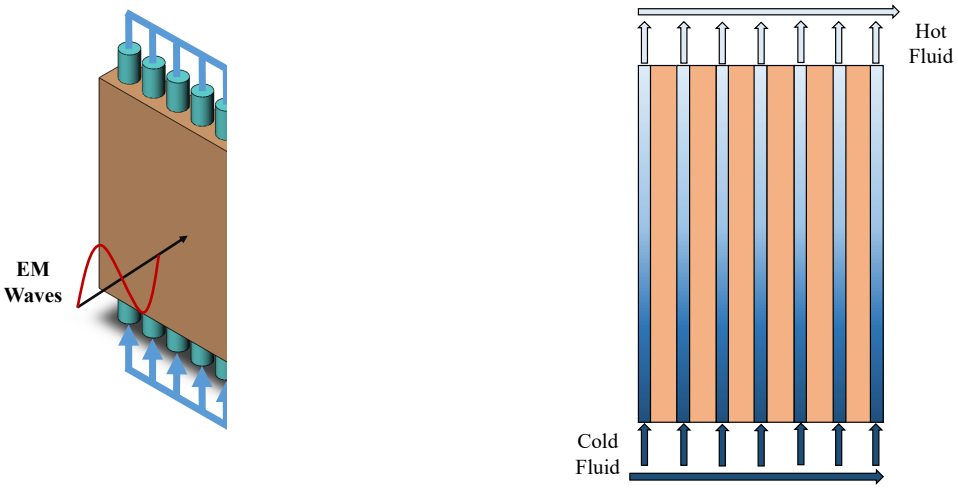

(a) (b)

Figure 1.1: (a) 3D simple parallel flow, and (b) 2D simple parallel flow heat exchanger.

Computational models may help clarify complicated interaction between nonlinear phenomena which might be difficult to comprehend and control experimentally. This raises demand on multiphysics models that are capable of adequately simulating all essential effects occurring in MHEs. A numerical model of a MHE requires simultaneous solution to multiple differential equations characterizing different physical phenomena, which in turn increases number of degrees of freedom involved in the complete solution. Since the nonlinear event of thermal runaway emerges due to the temperature dependent loss factor, spatial discreatizarion of the geometry must be able to capture decaying nature of the electric field along with exponential growth of the local temperature. As a result, the size of the global matrix becomes very large, i.e., a very large system of linear equations is needed to be solved at every time step. Thus, multiphysics modeling becomes complicated and requires heavy computational resources.

An example of generic heat exchangers found in practice are shown in Figure 1.1. In such heat exchangers, fluid flow is incorporated in order to effectively extract heat energy from the interfacing solid so as to achieve heating of the fluid or cooling of the heated solid.

Such an assembly of alternate fluid and solid layers can be considered as the structure of a simple MHE where heating of the solid layers is achieved by impinging MW radiations. As modeling of an MHE is computationally intensive, we take a simple three layered (fluid-solid-fluid) laminate system mimicking a MHE as a paradigm to understand the operation of MHE. Further, we consider parallel flow type of MHE to take advantage of symmetry of the structure.

In order to make multiphysics model manageable, we reduce total number of degrees of freedom by considering a 2D geometry. Size of the mesh elements used to discretize the geometry is dependent on the wavelength of EM waves. At higher frequency, the wavelength of EM waves becomes very small, and thus, a very small element size is required. In order to reduce requirement of higher number of mesh elements, we set the operating frequency of EM wave to be 2.45 GHz, i.e., one of the ISM frequencies widely used in microwave heating processes.

The study of mechanisms involved in a MHE is also possible with analytical models that simplify the system of coupled nonlinear governing equations into a solvable systems of differential equations. Such models rely on many assumptions in terms of the geometry, external operating conditions, material parameters, etc. Even though analytical models allow us to understand physics involved in the operation of MHE at relative low or negligible computational resources, they might not be able to reproduced a MHE which is exposed to actual operating conditions; e.g., the model of Gaone et al. [12] is limited to 1D analysis. In addition, since MHEs are still in developing stage, numerical models can help engineers to decide on design parameters such that higher thermal efficiency would be achieved. With these motivations in mind, this Thesis is focused on computational modeling of a 2D triple-layered MHE.

1.2 Modeling Microwave Heating

In order to formulate corresponding models, we need to identify the governing equations and describe the physical mechanisms through which energy is transferred from the EM

wave to the moving fluid. When EM waves are incident on a lossy material, some of the incident energy is reflected from the surface of the lossy material due to mismatch between material properties, some energy is transmitted through the material, and remaining energy is absorbed in the medium which gets converted into heat energy. We know that EM heating occurs due to two different sources; ohmic heating due to leakage currents that are produced due to time varying electric field, and dielectric heating due to rotating electric dipole moments. We define effective electrical conductivity σ_{eff} such that it takes into account heating due to both of the mechanisms. Electric energy that is absorbed by the lossy material generates a volumetric heat energy source given as

$$Q = \frac{1}{2}\sigma_{eff}|\vec{E}|^2, \tag{1.1}$$

where Q is EM power loss density, σ_{eff} is effective electrical conductivity of the medium, and $\vec{E}$ is the electric field.

Evolution of temperature is given by the heat equation heat equation, which describes energy conservation per unit volume given as

$$\rho c_p \left(\frac{\partial T}{\partial t} + \vec{u} \cdot \nabla T\right) = \nabla \cdot (K \nabla T) + \frac{1}{2}\sigma_{eff}|\vec{E}|^2, \tag{1.2}$$

where ρ is density of the material, c_p is specific heat of the material, T is the temperature, $\vec{u}$ is the fluid velocity, and K is thermal conductivity of the material. The first term on the left hand side represents energy absorbed by the material to increase its temperature, second term on the left-hand side represents energy transferred by convection due to the fluid flow, while the terms on the right-hand side represent the heat conduction, and the power generated by the conversion of EM waves to thermal energy.

The nature of the fluid flow can be understood by the Navier-Stokes equations, that are derived by applying conservation of mass and momentum to a differential control volume.

Incompressible Navier-Stokes are given by

$$\nabla \cdot \vec{u} = 0, \tag{1.3}$$

$$\frac{\partial \vec{u}}{\partial t} + \vec{u} \cdot \nabla \vec{u} = -\frac{\nabla P}{\rho} + \nu \nabla^2 \vec{u}, \tag{1.4}$$

where P is fluid pressure, and ν is kinematic viscosity. Equation (1.3) suggests that fluid mass is conserved, and (1.4) suggests momentum conservation. In our modeling descriptions below, we let $\vec{u} = \vec{0}$ and a constant P to represent a rigid solid dielectric medium.

The nature of electromagnetic waves is understood by Maxwell's equations. Gauss' law is given as

$$\begin{aligned} \nabla \cdot \vec{D} &= 0, \\ \nabla \cdot (\epsilon \vec{E}) &= 0, \end{aligned} \tag{1.5}$$

where $\vec{D} = \epsilon \vec{E}$ is electric flux density, and ϵ is permittivity of the medium. In another words, Gauss's law suggests that the electric flux leaving a volume is proportional to the charge inside. In our modeling considerations we assumes enclosed charge to be zero.

Gauss' law of magnetism states that there is no magnetic monopole, and is formulated as

$$\begin{aligned} \nabla \cdot \vec{B} &= 0, \\ \nabla \cdot (\mu \vec{H}) &= 0, \end{aligned} \tag{1.6}$$

where $\vec{B} = \mu \vec{H}$ is magnetic flux density, μ is permeability of the material, and $\vec{H}$ is magnetic field.

Faraday's law conveys that time varying electric field produces time varying magnetic field, and is given as

$$\begin{aligned} \nabla \times \vec{E} &= -j\omega \vec{B}, \\ &= -j\omega\mu \vec{H} \end{aligned} \tag{1.7}$$

where $\omega = 2\pi f$ is angular frequency of EM waves, f is frequency of EM waves.

Ampere's law states that oscillating magnetic field produces time varying electric field, and is given as

$$\begin{aligned} \nabla \times \vec{H} &= \vec{J} + j\omega\vec{D}, \\ &= \sigma\vec{E} + j\epsilon\omega\vec{E}. \end{aligned} \tag{1.8}$$

where and $\vec{J} = \sigma\vec{E}$ is surface current density. Propagation of electromagnetic waves in any medium can understood by coupled interaction of (1.5), (1.6), (1.7), and (1.8). Taking curl of (1.7) we get,

$$\begin{aligned} \nabla \times \nabla \times \vec{E} &= -j\omega\nabla \times (\mu\vec{H}), \\ &= -j\omega(\nabla\mu \times \vec{H} + \mu\nabla \times \vec{H}). \end{aligned} \tag{1.9}$$

From (1.7), (1.8), and (1.9) we get

$$\begin{aligned} \nabla \times \nabla \times \vec{E} &= -j\omega\left(\nabla\mu \times \left[\frac{1}{-j\omega\mu}\nabla \times \vec{E}\right] + \mu[\sigma + j\epsilon\omega]\vec{E}\right), \\ \nabla(\nabla \cdot \vec{E}) - \nabla^2\vec{E} &= \nabla\mu \times \left(\frac{1}{\mu}\nabla \times \vec{E}\right) - j\omega\mu[\sigma + j\epsilon\omega]\vec{E}). \end{aligned} \tag{1.10}$$

From Gauss' law (1.5),

$$\begin{aligned} \nabla \cdot (\epsilon\vec{E}) &= 0, \\ \epsilon\nabla \cdot \vec{E} + \nabla\epsilon \cdot \vec{E} &= 0, \\ \nabla \cdot \vec{E} &= -\frac{1}{\epsilon}(\nabla\epsilon \cdot \vec{E}). \end{aligned} \tag{1.11}$$

From (1.10) and (1.11), we get

$$-\nabla\left(\frac{1}{\epsilon}\nabla\epsilon \cdot \vec{E}\right) - \nabla^2\vec{E} = \nabla\mu \times \left(\frac{1}{\mu}\nabla \times \vec{E}\right) - j\omega\mu[\sigma + j\epsilon\omega]\vec{E}. \tag{1.12}$$

Permittivity and permeability of any material is defined as $\mu = \mu' - j\mu''$ and $\epsilon = \epsilon' - j\epsilon''$. The imaginary part of the permittivity, also called as loss factor, constitutes in

electromagnetic losses due to rotating dipole moment. Similarly, magnetic losses are induced due to the imaginary part of the permeability. Since in our modeling we assume that all the materials do not undergo magnetic losses, which means that $\mu'' = 0$, and μ is characterized by a real value of μ'. We also assume that μ' is a constant, thus $\nabla\mu = 0$. Substituting these approximations in (1.12), we get

$$\begin{aligned}\nabla\left(\frac{1}{\epsilon}\nabla\epsilon\cdot\vec{E}\right)+\nabla^2\vec{E} &= j\omega\mu'(\sigma+j[\epsilon'-j\epsilon'']\omega)\vec{E},\\ &= j\omega\mu'(\sigma+j\epsilon'\omega+\epsilon''\omega)\vec{E},\\ &= -\omega^2\mu'\epsilon'\left(1-j\left[\frac{\sigma+\omega\epsilon''}{\omega\epsilon'}\right]\right)\vec{E}.\end{aligned} \tag{1.13}$$

Since we call $\sigma_{eff} = \sigma + \omega\epsilon''$, (1.13) becomes

$$\nabla\left(\frac{1}{\epsilon}\nabla\epsilon\cdot\vec{E}\right)+\nabla^2\vec{E}+\omega^2\mu'\epsilon'\left(1-j\left[\frac{\sigma_{eff}}{\omega\epsilon'}\right]\right)\vec{E}=0. \tag{1.14}$$

We also consider temperature dependent electrical conductivity electric field is also a function of temperature, and (1.14) becomes

$$\nabla\left(\frac{1}{\epsilon}\nabla\epsilon\cdot\vec{E}(T)\right)+\nabla^2\vec{E}(T)+\omega^2\mu'\epsilon'\left(1-j\left[\frac{\sigma_{eff}(T)}{\omega\epsilon'}\right]\right)\vec{E}(T)=0. \tag{1.15}$$

Since $\mu' = \mu_r\mu_0$ and $\epsilon' = \epsilon_r\epsilon_0$, where ϵ_0 and μ_0 are the permittivity and permiabilty of the free space, and $c = \frac{1}{\sqrt{\mu_0\epsilon_0}}$, where c is the speed of EM waves in free space. We can write (1.15) as

$$\nabla\left(\frac{1}{\epsilon}\nabla\epsilon\cdot\vec{E}(T)\right)+\nabla^2\vec{E}(T)+k_0^2\mu_r\left(\epsilon_r-j\left[\frac{\sigma_{eff}(T)}{\omega\epsilon_0}\right]\right)\vec{E}(T)=0, \tag{1.16}$$

Where $k_0 = \frac{\omega}{c}$ is wave number of the free space. Therefore, MW heating of the considered medium is characterized by simultaneous solution of (1.2), (1.3), (1.4), and (1.16).

These governing equations can be solved when appropriate boundary conditions are applied. Volumetric heat generated during microwave heating is lost to the surrounding mainly

via two different modes; convective heat transfer and radiation heat transfer. Combined modes of heat losses at the respective boundaries are formulated as

$$-K\frac{\partial T}{\partial x} = h(T - T_A) + \xi\sigma_b(T^4 - T_A^4), \tag{1.17}$$

where h is the heat transfer coefficient between surrounding and the respective boundary, ξ is the emissivity coefficient of the surface, σ_b is the Stefan-Boltzmann Constant, and T_A is the ambient temperature. Whenever adiabatic conditions are maintained, i.e., when there is no heat losses at the boundary, then (1.17) becomes

$$-K\frac{\partial T}{\partial x} = 0. \tag{1.18}$$

A fluid flow is usually driven by the pressure difference between two regions (or a fluid with velocity u creates a pressure difference). When solving (1.4), we either need to specify fluid pressure or fluid velocity at the inlet and the outlet of the channel. In our modeling approaches in this thesis, whenever a fluid is in contact with solid surfaces, we assume no slip boundary conditions (as we are assuming that the laminar boundary layer is already developed i.e. hydrodynamically fully developed fluid flow) at the interfaces. Mathematically at no slip boundary, velocity of the fluid must be zero, i.e.,

$$\vec{u} = 0. \tag{1.19}$$

Boundary conditions while solving the Maxwell's equations (1.16) are derived by considering time dependent integral form of the Maxwell's equation (Pozar in [13]). It can be then deduced that normal components of $\vec{D}$ and $\vec{B}$, and tangential component of $\vec{E}$ and $\vec{H}$ are continuous across the dielectric interface. Mathematically speaking,

$$\hat{n} \cdot \vec{D_1} = \hat{n} \cdot \vec{D_2}, \tag{1.20}$$

$$\hat{n} \cdot \vec{B_1} = \hat{n} \cdot \vec{B_2}, \tag{1.21}$$

$$\hat{n} \times \vec{E_1} = \hat{n} \times \vec{E_2}, \tag{1.22}$$

$$\hat{n} \cdot \vec{H_1} = \hat{n} \cdot \vec{H_2}, \tag{1.23}$$

where n is unit vector pointing outwards at the interface. Therefore, simultaneous solution of governing equations when subjected to boundary conditions described above describes the process of MW heating.

1.2.1 MW Heating of a Solid Medium

In this section, we discuss the literature on the modeling of microwave heating of solid lossy medium. In the absence of fluid flow, $\vec{u}$ is zero, and MW heating is governed by (1.2) and (1.16). The first mathematical model studying MW heating of a 1D lossy ceramic slab was developed by Kriegsmann in [14]. While formulating this model, it was assumed that a very thin slab ceramic slab undergoes an EM illumination. The lossy layer was also assumed to be mostly insulated at the boundaries, and dominant mode of heat loss was through radiation heat transfer at the boundaries. For approximating temperature and electric field profiles, Kriegsmann in [14] assumed asymptotic expansions in term of convective heat losses at the boundaries. Since it was assumed that the dielectric slab is very thin and the convective heat loss at the boundaries is also small, spatial dependence of temperature and electric fields were conveniently dropped out, and resultant governing equation became a time dependent non linear ordinary differential equation (ODE), which is also referred as the amplitude equation in this work. The steady-state solution of the amplitude equation allowed the author to reconstruct incident power as a function of average steady state temperature, which is given as

$$P = \frac{v_0^* + \gamma[(v_0^* + 1)^4 - 1]}{f(v_0^*)||u_0||^2}, \tag{1.24}$$

where P is non dimensional form of incident power, v_0^* is non dimensional form of temperature, γ is radiation equivalence of the Biot number, $f(v_0^*)$ is a non dimensional electrical conductivity as a function of temperature, and u_0 is non dimensional electric field.

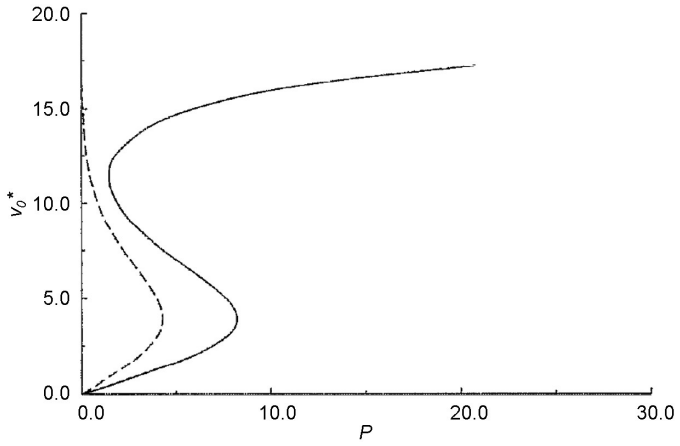

Figure 1.2: Power response curve for a very thin domain with the assumption of small Biot number, and exponential electrical conductivity model; P is non dimensional form of incident power, v_0^* is non dimensional form of temperature (Kriegsmann in [14]).

The plot of average steady state temperature versus power from (1.24) is called the power response curve, also known as S-curve. It shows how steady-state temperature solution varies with incident power. It is seen from Figure 1.2 that steady-state temperature is a multivalued function of the incident power. Depending on initial conditions (temperature), multiple steady-states are possible.

Extensions of this approach have been used in microwave-enhanced chemical vapor infiltration applications (Tilley and Kriegsmann in [15]) and in the microwave heating of laminate materials (Kriegsmann and Tilley in [16], Pelesko and Kriegsmann in [17]). All of the previous mathematical models imply that temperatures during thermal runaway are very high and difficult to control, and usually results in material damage due to mechanical failures, such as through thermal expansion or melting.

Very recently, a model for a triple layer laminate structure (Figure 1.3), developed by Gaone et al. in [12]. This work suggested that when an electric field resonance is achieved in the lossy layer, power response curve acquires another middle branch and becomes an SS-curve. Gaone et al. in [12] showed that when plane polarized waves are symmetrically and normally incident on the laminate, conditions analogous to Bragg interference occur for a fixed loss factor in the middle layer. For the loss factor depending on temperature, a

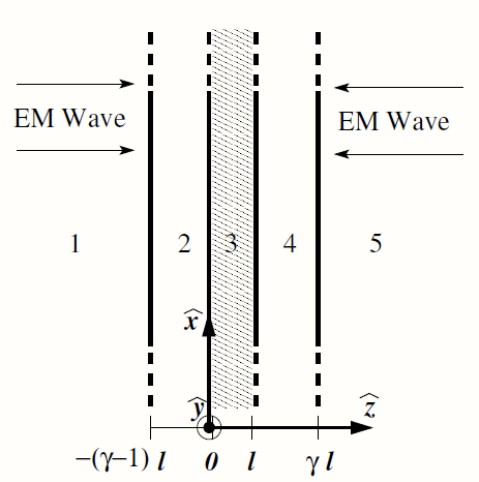

Figure 1.3: Three-layer laminate subjected to symmetric electromagnetic heating: regions 1 and 5 are free space, layers 2 and 4 are lossless dielectrics, layer 3 is a lossy dielectric (Gaone et al. in [12]).

new stable steady-state solution corresponding to resonance conditions, whose equilibrium temperature is significantly elevated, but prevents the occurrence of high temperatures during thermal runaway. SS curves are shown in Figure 1.4; we see that temperature during thermal runaway in lossy material may be within controllable range. Gaone et al. in [12] also suggested that a resonance of electric field, necessary to produce SS-curve, occurs when the width of the outer layers is an odd multiple of quarter wavelengths, $l(\gamma-1) = (2m-1)\lambda_2/4$, and the width of the lossy layer is an odd multiple of half wavelengths, $l = (2n-1)\lambda_3/2$, for $m, n = 1, 2, 3, ...$

Numerical modeling of microwave heating of a solid medium has been carried out by Clemens et al. in [18]. This study was focused on finding out the effect of electric field distribution, frequency, sample size, and dielectric properties on temperature distribution. Finite difference time domain (FDTD) method was used to solve Maxwell's equations, and heat transport equations were solved by implicit finite difference method. It was concluded that strong heating can be achieved when electric field resonance is achieved. An FDTD model developed by Yakovlev et al. in [19] was capable of capturing the effect of thermal runway in Zirconia. The objective of this work was to predict the behavior of high tempera-

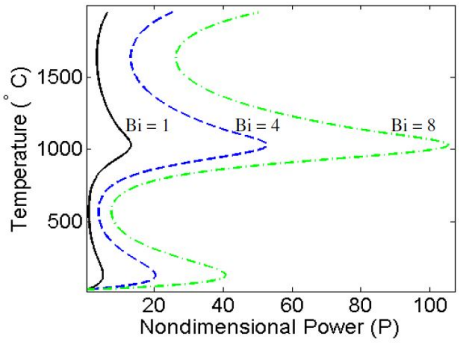

Figure 1.4: SS-shaped power response curve for triple a layered laminate structure with different Biot numbers developed by Gaone et al. in [12].

ture microwave processing of ceramics so as to optimize process parameters before working on the experimental development of new processes. This study demonstrated that heating rate and temperature patterns strongly depend on whether the system is fed at resonance, and the time at which runaway occurs was also predicted by the model.

In Chapter 2 of the thesis, we extend the approach of Gaone et al. in [12]. We validate a 2D numerical model of a triple layer laminate undergoing MW with the model of Gaone et al. in [12]. The latter model assumed a very thin triple layer laminate system and did not consider spatial dependence of electric field and temperature. However, numerical model in Chapter 2 overcomes this drawback by considering spatial dependence.

1.2.2 MW Heating of a Fluid Medium

In this section, we discuss numerical models for MW heating of a fluid medium reported in the literature. When MW heating of a Newtonian incompressible fluid medium is considered equations (1.2), (1.3), (1.4), and (1.16) are solved simultaneously in order to study the heating process. However, the governing equations are not directly solvable mathematically due to highly complicated nonlinear coupling, the system of equations can be effectively solved numerically.

A numerical model of MW heating of a static lossy fluid was developed by Ratanadecho et al. in [20]. The numerical technique of finite control volume method was used to

solve the system of equations. It was concluded that dielectric loss factor has an effect on temperature distribution. The model of Ratanadecho et al. in [20] considered temperature dependent dielectric properties of the water and saline water. Initially, heat generation was calculated by assuming uniform properties at the initial temperature. The electromagnetic calculation was performed until a sufficient period, typically 30,000 time steps, is reached, and RMS value of the electric field at each spatial point was obtained. The microwave power absorption at each point was calculated and used to determine temperature. Electromagnetic properties were recalculated at this temperature and used in next iteration. All these steps were repeated until required heating time is reached.

The numerical simulation of forced convection through a rectangular duct subjected to microwave heating was studied by Zhu et al. in [21]. In this model, Maxwell's equations were solved using the FDTD method and transient temperature and flow patterns were simulated using the finite volume method. This numerical model assumed the flow to be non-Newtonian, and also assumed temperature dependent dielectric properties. Forced convection in a rectangular applicator tube which is placed inside a single mode resonating cavity was simulated. Flow in the applicator tube was assumed hydrodynamically fully developed. This work was aimed to determine uniformity of heat generation in the fluid, and find out its relation with dielectric properties, and loss tangent. This model considered MW heating of the fluid in a resonating cavity, and also showed that size of the cavity and incident power levels also have an effect on temperature profiles.

Numerical models of continuous flow microwave heating system modeled with ANSYS Multiphysics are developed by Sabilov et al. in [22], Salvi et al. in [23], and Salvi et al. in [24]. Since these models considered Newtonian and incompressible fluid flow, FLOTRAN CFD module in ANSYS was used to solve (1.2),(1.3) and (1.4), and high frequency electromagnetic module was used to solve (1.16). These models did not consider temperature dependent dielectric losses. One of objectives of these models was to understand MW heating of a fluid medium itself, and also to find out effects of material properties and operating conditions on heating mechanisms. These model showed capability of ANSYS Multiphysics

in modeling microwave heating of continuous fluid medium. In addition, COMSOL Multiphysics was used to model continuously flowing water by Salvi et al. in [25] and by Muley and Bolder in [26]. Both of these models considered temperature dependent thermal as well as dielectric properties.

All of the models discussed in this section were mainly focused on modeling MW heating of a fluid medium itself. Since the end applications of these models were to replicate applications in food and chemical processing, they were not aimed to understand heat transfer between MW heated solid and flowing fluid phenomenon necessary for heat extraction. In addition, no model captured the phenomenon of thermal runaway in a solid lossy medium when fluid flow is also present. 2D models of MHE developed in this thesis do not consider a lossy fluid, and hence MW heating the fluid was not considered. However, models reported in the literature demonstrate the capability of commercial software packages to model microwave heating.

1.3 Comparison of Commercial Numerical Packages

Use of commercial software in modeling microwave heating of a lossy fluid as well as solid medium has also been a popular choice. QuickWave has been found to be one of the most efficient packages when it comes to microwave heating of a solid medium. However, Quickwave lacks capability of simulating microwave heating of fluid flow, and hence cannot simulate the full problem that describe a MHE. Yakovlev in [27] and [28] suggested that whenever fluid flow is incorporated along with MW heating, COMSOL Multiphysics and ANSYS Multiphysics have been found applicable.

A critical comparison of capabilities of COMSOL Multiphyisics and ANSYS Multiphysics in modeling MW heating of continuous flowing was carried out by Salvi et al. in [29]. ANSYS uses different mesh elements for different physics, whereas COMSOL uses the same mesh elements for different physics. Salvi et al. in [29] and Demjanenko et al. in [30] reported that the issue of element mismatch during multiphysics coupling was prevalent, and appears to be a potential source of rounding errors. COMSOL provided a flexible model

setup, whereas ANSYS required coupling incompatible elements to transfer load between electromagnetic, fluid flow, and heat transport modules.

In addition, we carried out studies on comparison of COMSOL and ANSYS for solving canonical problems in heat transfer, fluid mechanics, and electromagnetics phenomena. We first solved canonical problems using software packages, and then compared its results with theoretical results. Since the QuickWave can model electromagnetic phenomenon very accurately, we referred to a solution produced by QuickWave at a very fine discretization as the benchmark solution, and results from EM analysis were compared with this benchmark solution. The details of these studies are placed in Appendix, and only important results and conclusions directly relevant to the topic are included in the main body of the Thesis. We found that COMSOL had advantages over ANSYS as it allows coupling between same mesh elements. Therefore, we use COMSOL Multiphysics, a finite element method (FEM) based software for further analysis.

1.4 Motivation and Scope of This Work

The rate at which MW energy is absorbed by a lossy material is dependent on the loss factor. For many practical materials, it is dependent on temperature and increases exponentially with temperature. Such nonlinearity leads to a positive feedback loop causing thermal runaway. The theoretical description of thermal runaway was given for a single dielectric slab (Kriegsmann in [14]) and a three-layer geometry (Pelesko and Kriegsmann in [17]), in terms of a non-dimensional ratio of thermal losses to MW power, called the power response curve. It shows how the steady-state temperature of the material depends on the MW power. The multi-valued profile of this curve (see Figure 1.4 (a)) implies that a system can reach different steady-state temperatures when initial temperatures are different.

Temperatures at thermal runaway are usually very high and difficult to control, and usually damage the material itself. As a mathematical model developed by Gaone et al. in [12] for a triple-layer laminate shows, for particular values of the layer width and complex permittivity, the S-curve acquires another (third) stable branch and becomes the SS-curve

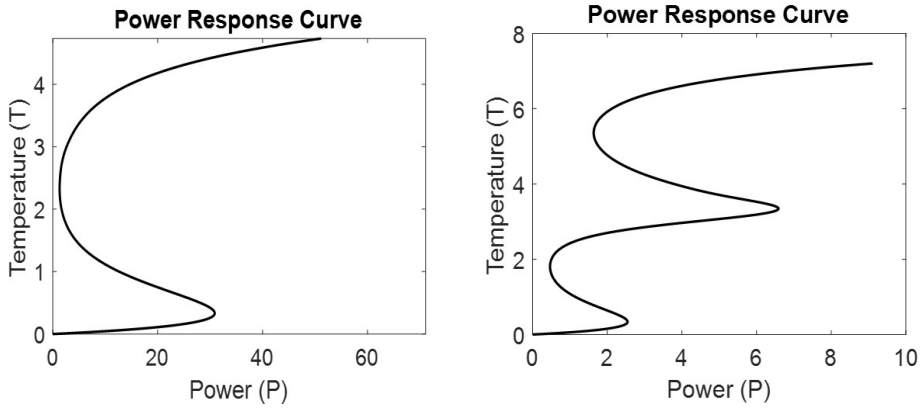

(a) (b)

Figure 1.5: (a) Generic S-curve (Kriegsmann in [14]) and (b) SS-curve (Gaone et al. in [12]) for non-dimensional power

(Gaone et al. in [12]). A generic SS-curve is shown in Figure 1.5 (b). This suggests a possibility of a new technique of keeping thermal runaway under control and efficiently converting electromagnetic energy into other usable forms of heat. Such lossy media can be either porous materials or materials with channels to accommodate fluid flow for absorbing heat.

Thermal runaway has been studied experimentally (Wu in [31], Chandran et al. in [32]) and numerically (Yakovlev et al. in [19]). However, numerical models reproducing power response curve have not been reported. In the present thesis we address this drawback in chapter 2. We develop a multiphysics model capturing the behavior of a power response curve for the three-layered structure imitating one of the MHE's basic setups. We validate this model with the 1D mathematical model developed by Gaone et al. [12]. Due to differences in underlying assumptions implied by both the models, disparities in results were observed. As a part of validation, we also numerically verify the disparities.

After validating the model, we extend the approach in Chapter 3 by incorporating fluid flow in order to accommodate heat extraction. We show that high thermal efficiency is achieved when thermal runaway is occurred. In Chapter 4 of the Thesis, we discuss important insights that were gained through the computational modeling in this work, and also discuss how our findings can help design an efficient MHE.

Chapter 2

Effects of External Energy Loss on the Power Response Curve of a Lossy Triple-layer System Without Fluid Flow

We consider a 2D, triple-layered structure as shown in Fig. 2.1. This setup may be seen as a model of a MHE with absorbing (ceramic) layer surrounded by pure dielectric fluid channels. In this Chapter, we assume that there is no fluid flow in the lossless layers 2 and 4. We first check the validity of the numerical model through a comparison of its output with the results from a related 1D mathematical model. Once the validation is done, the effects of heat transfer with fluid flow in regions 2 and 4 of this system is investigated in Chapter 3.

We have plane waves incident from both sides with the assumption that the incoming waves are polarized along the Y-direction and traveling in the X-direction. Time average power density of the incident plane wave is given by

$$P_{av} = E_0^2/2\eta, \tag{2.1}$$

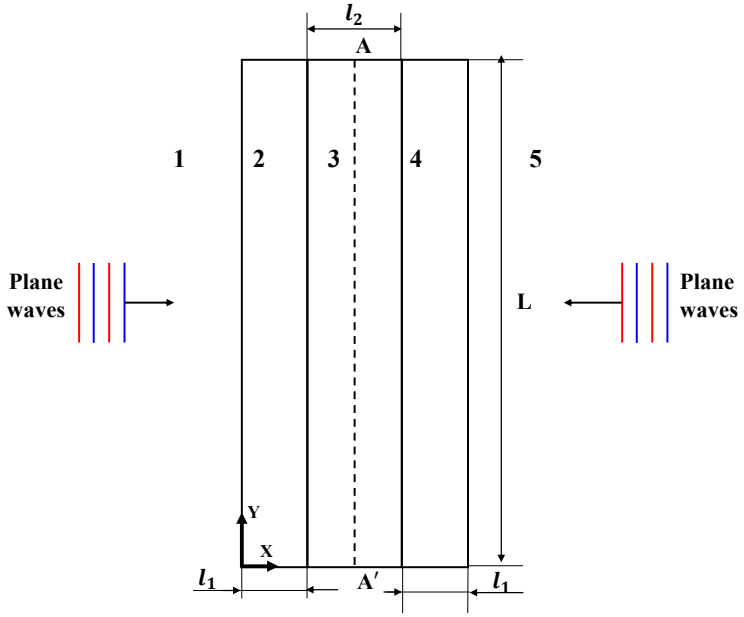

Figure 2.1: Geometry of the three layered system subjected to electromagnetic heating (symmetric about AA'). Medium 1 and 5 are free space, layer 2 and 4 are lossless, layer 3 is a lossy dielectric.

where E_0 is amplitude of the incident electric field, and η is characteristic impedance of free space. In order to achieve electric field resonance necessary to produce the SS-curve, we need to satisfy following conditions (Gaone et al. in [12])

$$l_1 = \frac{n_1 \lambda_2}{4}, \text{ and } l_2 = \frac{n_2 \lambda_3}{2},$$

where n_1 and n_2 can be any odd number, i.e., $1, 2, 3, ...$, λ_2 and λ_3 are wavelength in region 2 and 3, respectively. With different combinations of n, we can observe different resonating modes of electric field. We consider three different electric field modes, and corresponding dimension used in this model are as shown in Table 2.1.

	n_1	l_1 [mm]	n_2	l_2 [mm]
Mode 1	3	10.89	1	23.65
Mode 2	5	18.15	3	70.95
Mode 3	7	25.41	5	118.27

Table 2.1: Layer widths necessary to produce SS-curve (according to resonance conditions by Gaone et al. in [12]).

2.1 Governing Equations

We construct a numerical model in *COMSOL Multiphysics* capable of solving a coupled system involving Helmholtz's and heat equations. We introduce non-dimensional variable $\tilde{E} = \vec{E}/E_0$, where $\vec{E}$ and $\tilde{E}$ are dimensional and non-dimensional forms of the electric field, respectively. These equations are given by

$$\nabla^2 \tilde{E}_i + k_0^2(\epsilon'_{ri} - j\frac{\sigma_i(T_i)}{\omega\epsilon_0})\tilde{E}_i = 0, \tag{2.2}$$

$$\frac{\partial T_i}{\partial t} = \alpha\nabla^2 T_i + \frac{Q_i}{\rho_j c_{p_i}}, \tag{2.3}$$

$$Q_i = \sigma_i(T_i)|E_0\tilde{E}_i|^2, \tag{2.4}$$

where i represents the region of solution, $k_0 = \frac{\omega}{c}$ is wavenumber of free space, ω is angular frequency, c is speed of EM wave in free space, ϵ_0 is permittivity of free space, ϵ'_r is relative permittivity, T is temperature, $\sigma(T)$ is temperature dependent electrical conductivity, α is thermal diffusivity, Q is electromagnetic power loss density, ρc_p is volumetric heat capacity. We solve (2.2) for $i = 1, ...5$, (2.3) for $i = 2, 3, 4$, and (2.4) for $i = 3$.

2.2 Boundary Conditions

As region 1 is free space, for $x < 0$,

$$\tilde{E_1}(x) = e^{jk_0 x} + \tau e^{-jk_0 x}, \tag{2.5}$$

where $\tilde{E_1}$ is electric field in region 1, τ is the reflection coefficient between regions 1 and 2. At the boundary between regions 1 and 2 i.e at $x = 0$, we have C^0 and C^1 continuity of the electric field; that yields

$$\begin{aligned} \tilde{E_1}(0) &= \tilde{E_2}(0), \\ \frac{\partial \tilde{E_1}(0)}{\partial x} &= \frac{\partial \tilde{E_2}(0)}{\partial x}, \end{aligned} \tag{2.6}$$

where $\tilde{E_2}$ is electric field in region 2. From (2.5) and (2.6), we can say that

$$\tilde{E_1}(0) = 1 + \tau = \tilde{E_2}(0), \tag{2.7}$$

and

$$\frac{\partial \tilde{E_1}(0)}{\partial x} = jk_0(1 - \tau) = \frac{\partial \tilde{E_2}(0)}{\partial x}. \tag{2.8}$$

Combining (2.7) and (2.8) and eliminating reflection coefficient τ we get

$$\frac{\partial \tilde{E_2}}{\partial x} + jk_0\tilde{E_2} = 2jk_0 \quad \text{at} \quad (x = 0, y). \tag{2.9}$$

We maintain C^0 and C^1 continuity of the electric field at the interfaces between regions. Which means that

$$\begin{aligned} \tilde{E_2}(l_1) &= \tilde{E_3}(l_1), \\ \frac{\partial \tilde{E_2}(l_1)}{\partial x} &= \frac{\partial \tilde{E_3}(l_1)}{\partial x}. \end{aligned} \tag{2.10}$$

Since a symmetry condition is assumed at AA', we have,

$$\frac{\partial \tilde{E_3}}{\partial x} = 0 \quad \text{at} \quad (x = l_1 + \frac{l_2}{2}, y). \tag{2.11}$$

As we want to maintain a uniform electric field in the Y-direction, we apply

$$\frac{\partial \tilde{E_i}}{\partial y} = 0 \quad \text{at} \quad (x, y = 0) \text{ and } (x, y = L). \tag{2.12}$$

Medium	ϵ_r	$\sigma_{eff}(T)$[S/m]	K [W/mK]	ρc_p [J/m^{3}K]
1, 5	1	0	-	-
2, 4	71	0	0.6	435
3	6.69	$0.001e^{\left[\frac{T-300}{100}\right]}$	0.6	435

Table 2.2: Material properties of triple-layered laminate system.

Similarly for heat equation, we set

$$-K_2\frac{\partial T_2}{\partial x} = h[T_2 - T_A] \quad \text{at} \quad (x = 0, y), \tag{2.13}$$

where K_2 is thermal conductivity of region 2, T_2 temperature in region 2, $T_A = 300K$ is ambient temperature, and h is heat transfer coefficient at the respective boundary.

$$\frac{\partial T_3}{\partial x} = 0 \quad \text{at} \quad (x = l_1 + \frac{l_2}{2}, y), \tag{2.14}$$

In order to achieve uniform temperature in the y direction, we set

$$\frac{\partial T_i}{\partial y} = 0 \quad \text{at} \quad (x, y = 0) \text{ and } (x, y = L). \tag{2.15}$$

We also assume perfect thermal contact between the interfacing boundaries, so we can conveniently maintain C^0 and C^1 continuity. Therefore at the interfacing boundary C^0 and C^1 continuity is maintained at the interfaces between regions. That means

$$\begin{aligned} T_2(l_1) &= T_3(l_1), \\ \frac{\partial T_2(l_1)}{\partial x} &= \frac{\partial T_3(l_1)}{\partial x}, \end{aligned} \tag{2.16}$$

We also define the Biot number as $Bi = \frac{hl_2}{k_m}$, where k_m is the thermal conductivity of region 3. Initially, we assume $Bi = 0.5$, i.e., $h = 12.68\frac{W}{m^2K}$. In later simulations, we vary the Bi and graphically show the effect of spatially dependent temperature profiles.

2.3 Assumptions

Material properties used in computations below are chosen as shown in Table 2.2. In particular, volumetric heat capacity is considered to be small to ensure that thermal runaway occurs at lower power levels and considerably reduce computational cost of sweeping over the large power range. Temperature dependency of thermal parameters is not considered in this model, but left for future developments. ϵ_r and μ_r are also assumed to be temperature independent. All the materials used are assumed non-magnetic ($\mu_r = 1$). In addition, only the middle layer (material 3) absorbs MW energy, and the outer layers (materials 1, 2, 4, and 5) are considered lossless.

2.4 Solver and Convergence Criteria

Selection of a solver in COMSOL Multiphysics strongly depends on degree of non-linearity. Helmholtz's and heat equations are coupled with each other via temperature dependent non-linear electrical conductivity, which typically increases exponentially with the temperatures (Hill and Jennings in [6]) for many dielectric materials. Depending on initial guess, while solving non-linear steady state problems, COMSOL's default nonlinear steady state Newton-Raphson solver can fail to converge to desired solution [33]. As temperature is a multi-valued function, initial guess is uncertain, therefore, we use an implicit backward differentiation formula (BDF) based time dependent solver that discretizes time steps with backward differentiation formulas with order of accuracy varying from one (also know as the backward Euler method) to five. and steady state is assumed to be reached when absolute difference between average temperatures at previous and current time step falls below 10^{-6}.

BDF methods have been used for a long time and they are known for their stability. For solving nonlinear problems effectively, we use the default adaptive backward difference time stepping algorithm. Depending on temporal gradients of the fields, it automatically adjusts time step taken by the solver. The larger the gradients, the smaller the time step is. Since the time required for EM wave propagation is small compared to time required

for heat transfer and fluid flow, Helmholtz's equations are solved in frequency domain, and the time stepping algorithm is utilized when solving heat equations.

2.5 Meshing

The geometry is discretized using triangular elements, whose maximum size S_i is given by the Nyquist criterion (Sadiku in [34]):

$$S_i < \frac{\lambda_i}{2} = \frac{c}{2f\sqrt{\mu'_{ri}\epsilon'_{ri}}},$$

where λ_i is wavelength of the EM wave in corresponding region i. In other words, we need at lest two elements per wavelength. This criteria might be true while solving coupled Helmholtz and heat equations with temperature independent electrical conductivity. In our case, electrical conductivity increases exponentially with temperature. It means that skin depth is also decreasing with temperature. Therefore, at higher temperature we must resolve the spatial domain in such a way that we take into account diminishing nature of electric field. Therefore, we need to use mesh size comparable to skin depth of the material.

2.6 Computational Results

We now solve the model that is described in previous sections, and visualize spatially dependent steady state temperature profiles.

2.6.1 Critical Temperature

Figure 2.2 shows steady state spatially dependent temperature profiles generated by the numerical model. When incident power is 4,088 W/m^2, we see that maximum temperature is 416.1 K. As soon as the incident power is increased to $4,089$ W/m^2, we see a big jump in the temperature due to thermal runaway, see Figure 2.2 (b). Thus, we see that thermal runaway is triggered when maximum temperature reaches a critical temperature of 416.11

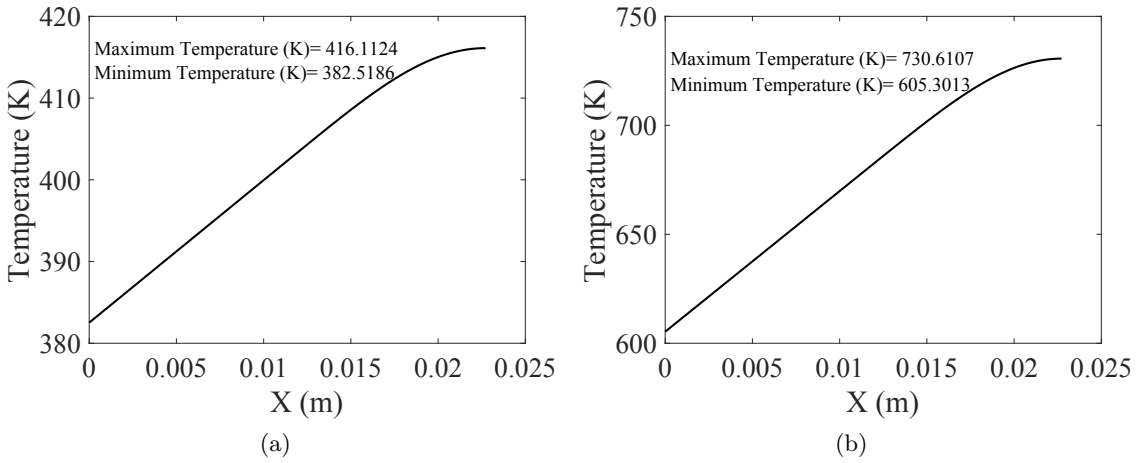

(a) (b)

Figure 2.2: Steady state temperature profiles along X-direction when incident power density is 4088 W/m^2 (a), and 4089 W/m^2 (b); initial temperature is 300 K.

K. The critical temperature is in accordance with the mathematical model of Gaone et al. in [12]; 416.5 K this confirms the functionality of the COMSOL model.

2.6.2 Comparison of Power Response Curve With Mathematical Model

Figure.2.3 shows the comparison of the power responses generated by the COMSOL model and the mathematical model of Gaone et al. [12]. Since the latter produces steady state average temperature as a multi-valued (depending on initial conditions) function of incident power, average temperature values are plotted against incident power when different initial conditions are maintained. The mathematical model (Gaone et al. in [12]) shows stable steady states as a solid line (branch AG and HM) and unstable states as a dashed line (branch GH). The transition between the lower (branch AG) and upper branch (branch HM) do not occur at the same power level. This hysteresis is confirmed by the COMSOL model (branch AC and branch FE) through increasing power with an initial temperature at 300 K (path ABCDE) and then by decreasing power with an initial temperature of 750 K (path EDFBA). Like our COMSOL model, the mathematical model (Gaone et al. in [12]) assumes uniform heating in the Y direction, but it applies asymptotics to a thin

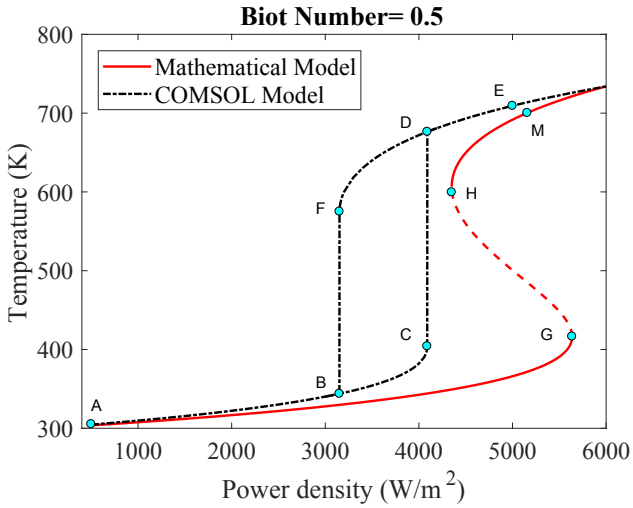

Figure 2.3: Comparison of low power regions of power response curves in the considered structure. Temperatures at points C, G, F, and H are 413.5 K, 416.5 K, 574.6 K, and 606.6 K respectively.

domain resulting in a time dependent ordinary differential equation of average temperature uniform in the X-direction. In contrast to this, the COMSOL model rigorously computes the temperature variation along the X-axis.

In order to investigate the reason behind differences seen in power response curves produced by the COMSOL and mathematical models, we apply the conservation of energy principle to the system at steady state, and find that

$$\int_0^{l_2} \frac{1}{2}|E_0^2 \tilde{E}_3(T_3)|^2 \sigma_3(T_3) dx = 2h(\tilde{T}_2 - T_A), \tag{2.17}$$

where $\tilde{T}_2$ is surface temperature at $X = -l_1$, $T_3(x)$ is temperature profile in region 3, and l_1 and l_2 are the widths of layers 2 and 3, respectively. For the COMSOL model, from (2.1) and (2.17), the input power density can be written as

$$P_1 = \frac{2h(\tilde{T}_2 - T_A)}{\eta \int_0^{l_2} |\tilde{E}_3(T_3(x))|^2 \sigma_3(T_3(x)) dx}. \tag{2.18}$$

Similarly, for the mathematical model, (2.1) and (2.17) can be simplified in terms of input

	Observed power density [W/m^2]	Observed $(P_2 - P_1)$ [W/m^2]	Calculated $(P_2 - P_1)$ [W/m^2]
Point C	P_1= 4088	1548	1548.55
Point G	P_2= 5636		
Point F	P_1= 3152	1199	1200.41
Point H	P_2= 4351		

Table 2.3: Comparison of critical transition powers.

power density as

$$P_2 = \frac{2h(\bar{T}_s - T_A)}{\eta|\tilde{E}_3(\bar{T}_s)|^2\sigma_3(\bar{T}_s)l_2}, \tag{2.19}$$

where $\bar{T}_s$ is average steady state temperature in the model (Gaone et al. in [12]). From (2.18) and (2.19), we can say that

$$P_2 - P_1 = \frac{2h(\bar{T}_s - \tilde{T}_2) - P_2P^*}{\bar{P}_1}, \tag{2.20}$$

where

$$\bar{P}_1 = \eta \int_0^{l_2} |\tilde{E}_3(T_3(x))|^2\sigma_3(T_3(x))dx,$$

$$\bar{P}_2 = \eta|\tilde{E}_3(\bar{T}_s)|^2\sigma_3(\bar{T}_s)l_2,$$

and

$$P^* = \bar{P}_2 - \bar{P}_1.$$

Numerical evaluation of (2.20) at the corresponding transition points on the SS-curve shown in Fig. 2.3 is given in Table 2.3.

2.6.3 Effect of the Biot Number on the Power Response Curve

From the COMSOL model, we observe that thermal runaway is triggered by maximum temperatures in the lossy layer. Global temperatures increase rapidly as soon as the local maximum temperature reaches a critical temperature. Effect of spatial dependence of electric field and temperature can be understood from (2.20). We see that as we increase the Biot number by increasing h, $(\bar{T}_s - \tilde{T}_2)$ also increases, which then increases differences in

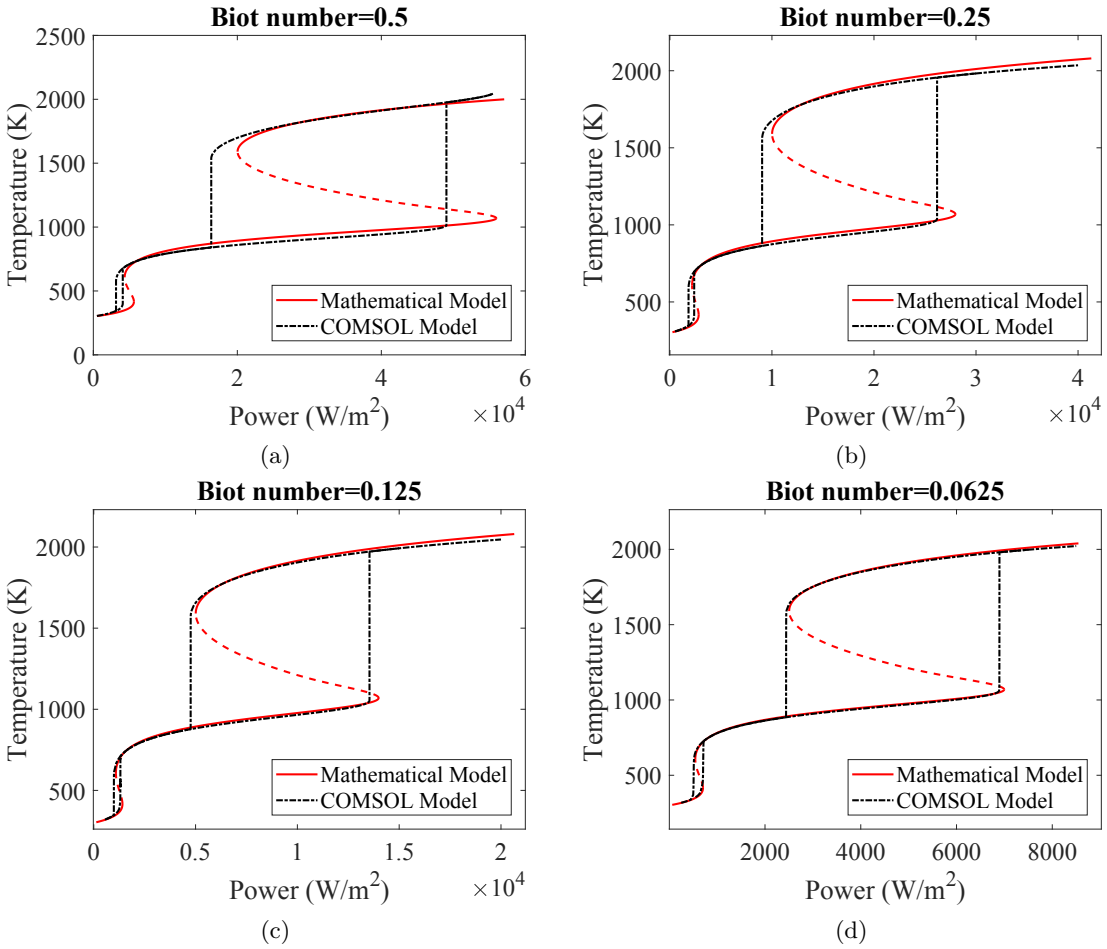

Figure 2.4: Comparison of the SS curves produced by the COMSOL and mathematical model (Gaone et al. in [12]) with (a) Bi = 0.5, (b) Bi = 0.25, (c) Bi = 0.125, and (d) Bi = 0.0625.

power response curves. Figure. 2.4 shows the comparison of SS-curves for different values of the Biot number. At smaller Biot number, external surfaces will behave like a thermal insulator, which makes temperature profile nearly uniform in the X-direction. Therefore, as we decrease the Biot number, differences in the power response curves given by the COMSOL and mathematical models keep on decreasing. On the other hand, when the Biot number is large, spatial temperature variation becomes important, therefore, differences in power responses increase. It is observed that for increasing values of the Biot number, critical transition power also increases, but transition temperature remains the same.

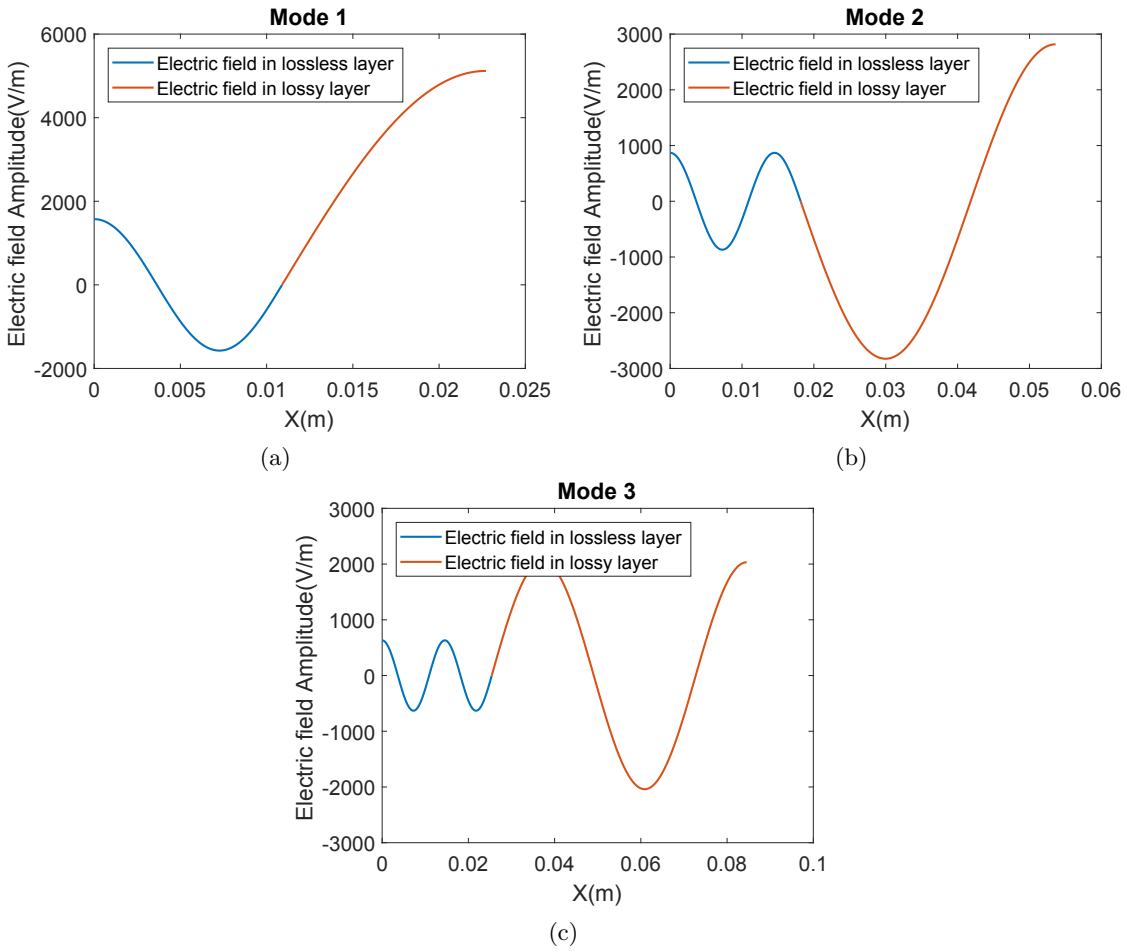

Figure 2.5: Electric field profiles for resonance (a) mode 1, (b) mode 2, and (c) mode 3 of electric field occurred in the lossy layer.

2.6.4 Effect of Resonance Modes on the Power Response Curve

As we are symmetrically irradiating the triple layered laminate structure with plane polarized microwaves, we can expect to observe standing wave pattern of the electric field. With the resonance criteria mentioned earlier, we see larger strength of the electric field in the lossy layer (in region 3). Spatially dependent electric field patterns corresponding to resonance modes given in Table 2.1 are visualized in Figure 2.5. We see that total EM energy losses in the ceramic layer are also increasing as we consider higher resonating modes of electric field.

Effect of considering spatially dependent temperature can also be understood from Fig-

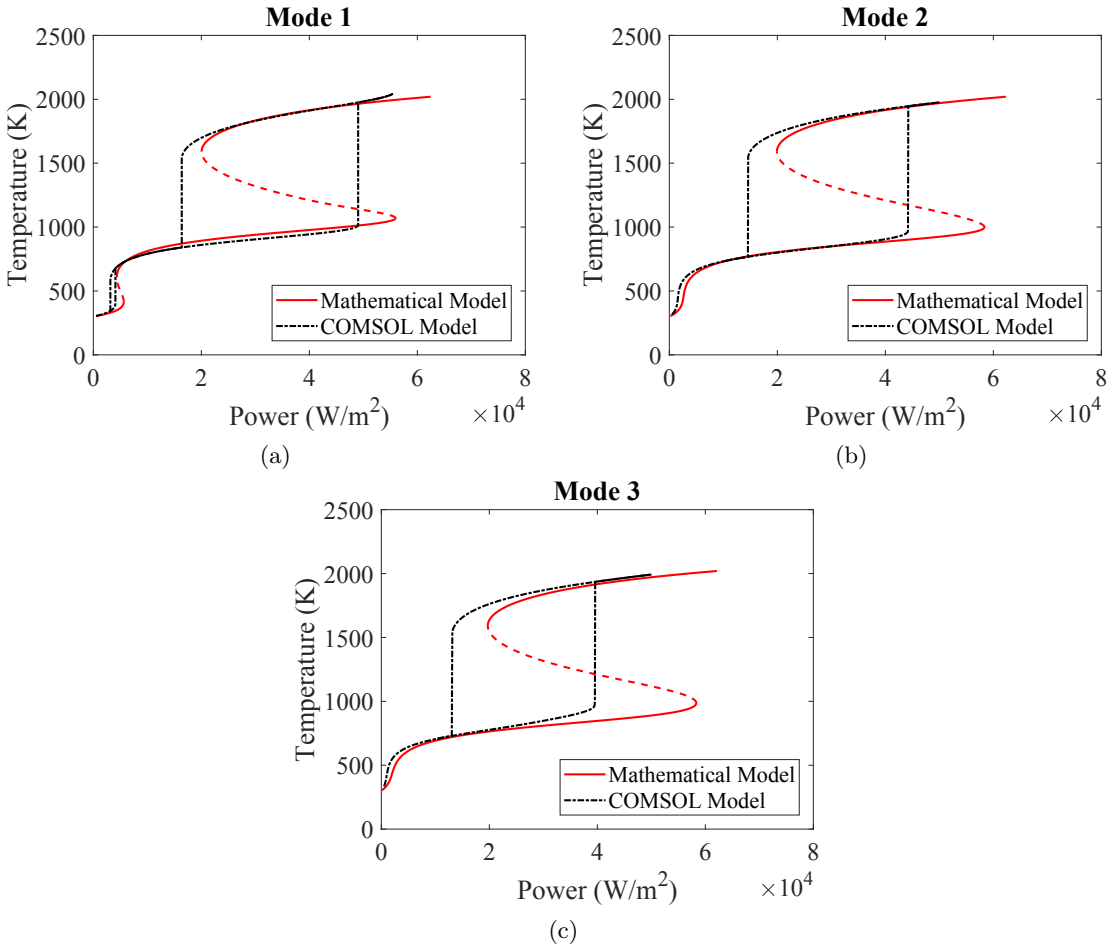

Figure 2.6: Power response curve corresponding to resonance (a) mode 1, (b) mode 2, and (c) mode 3 of electric field occurred in the lossy layer.

ure 2.6. Since we increase l_1 and l_2 according to the resonance criteria in order to achieve different resonating modes of the electric field, disparities in power response curves produced by COMSOL and mathematical models increases as we consider higher modes of operation.

2.7 Summary

We describe here a 2D numerical model which can solve non linear coupled Helmholtz and heat equations in a triple layered laminate. The model captures the S- and SS-profiles of the power response curve by considering spatial dependence of the temperature. This study

validates the 2D numerical model with the related 1D mathematical model. Differences seen in the results produced by both the models are attributed to underlying assumptions made by respective models. Thermal runaway, a non linear phenomenon where overall temperatures increase rapidly with a small increase in incident power, triggers when maximum temperature in the system reaches a critical value. External operating conditions, such as Biot number do not affect the critical temperature, but critical incident power increases with Biot number.

Chapter 3

Model of a Lossy Triple-Layered System With Fluid Flow

Since the validation of the numerical model without fluid flow is done in Chapter 2, in order to understand heat extraction from a MW heated ceramic, we now incorporate fluid flow along with symmetric MW heating of the lossy layer. We describe a 2D numerical model which solves coupled Helmholtz, continuity, momentum, and energy equations. We extend the approach of Chapter 2 by introducing a hydrodynamically fully developed Poiseuille flow in fluid carrying channels. A triple layer geometry mimicking a layered MHE is considered in the model. The scenario considered in this modeling approach is shown in Figure 3.1. Middle layer (region 3) is the lossy layer with temperature dependent loss factor, and region 2 and region 4 accommodate hydrodynamically fully developed Poiseuille flow.

As we assume that the incoming field is a plane wave, time average of the incident power density can be given by Poynting vector as

$$P_{av} = \frac{E_0^2}{2\eta}, \tag{3.1}$$

where E_0 is an amplitude of the incident electric field, η is the characteristic impedance of free space. Dimensions of the triple layer geometry are chosen according to resonance

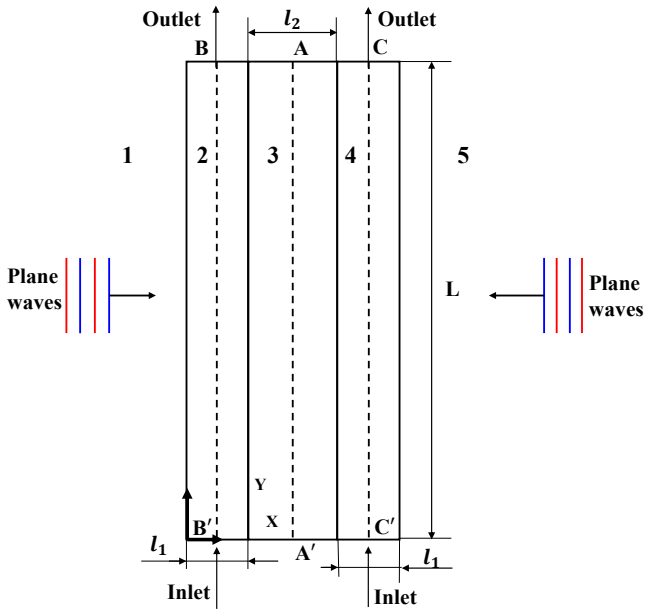

Figure 3.1: Geometry of the three layerd system subjected to electromagnetic heating (symmetric about AA'). Medium 1 and 5 are free space, layer 2 and 4 are lossless, layer 3 is a lossy dielectric; fully developed Poiseuille flow is introduced in region 2 and 4.

criteria given by Gaone et al. in [12].

$$l_1 = \frac{3\lambda_2}{4}, \text{ and } l_2 = \frac{\lambda_3}{2},$$

where λ_2 and λ_3 are wavelength in region 2 and 3, respectively. As the operating frequency in this model is 2.45 GHz, $l_1 = 10.89$ mm and $l_2 = 23.65$ mm. Initially we assume length of the fluid channel to be $L = 200$ mm, but later we vary the length of the fluid channel and visualize steady-state temperature solution.

3.1 Assumptions

Material properties used in this model are chosen as shown in Table 3.1. The convective heat transfer between the heated ceramic and fluid flow is dependent on volumetric heat capacity. In order to ensure that thermal runaway occurs at lower power levels so as to

Medium	ϵ_r	$\sigma_{eff}(T)$ [S/m]	α [m^2/s]	ρc_p [J/m^3K]	ν [m^2/s]
1, 5	1	0	-	-	-
2, 4	71	0	0.00137	435	0.0096
3	6.69	$0.001e^{\left[\frac{T-300}{100}\right]}$	0.00137	435	-

Table 3.1: Material properties considered for the model with fluid flow

save computational cost, we assume the volumetric heat capacity of the fluid is very small. We this assumption, heat energy extracted by the would also be small. If the volumetric heat capacity is increased, critical powers would also increase due to increased convection between fluid and the heated ceramic, thus in turn would lead to increased computational cost of sweeping over large power levels. We assume that the fluid is incompressible in nature, and does not undergo phase change phenomenon. Temperature dependent thermal and fluid properties are not considered in this model. ϵ_r and μ_r are also assumed to be temperature independent.

3.2 Governing Equations

We now construct a 2D COMSOL model capable of solving a coupled system involving Helmholtz, momentum, continuity, and energy equations. These equations are given by

$$\nabla^2 E_i + k_0^2 \left(\epsilon'_{ri} - j\frac{\sigma_i(T_i)}{\omega\epsilon_0} \right) E_i = 0, \tag{3.2}$$

$$\rho_i c_{p_i} \frac{\partial T_i}{\partial t} + \vec{u_i} \cdot \nabla T_i = K_i \nabla^2 T_i + \frac{1}{2}\sigma_i(T_i)|E_i|^2, \tag{3.3}$$

$$\frac{\partial \vec{u_i}}{\partial t} + \vec{u_i} \cdot \nabla u_i = -\frac{\nabla P_i}{\rho_i} + \nu_i \nabla^2 \vec{u_i}, \tag{3.4}$$

$$\nabla \cdot \vec{u_i} = 0, \tag{3.5}$$

where i represents the region of solution, E is the electric field, $k_0 = \frac{\omega}{c}$ is the wavenumber of free space, ω is angular frequency, c is the speed of EM wave in free space, ϵ_0 is permittivity of free space, ϵ'_r is relative permittivity, T is temperature, $\sigma(T)$ is temperature dependent electrical conductivity, K is thermal conductivity, ρc_p is volumetric heat capacity. $\vec{u_i}$ is

zero for region 3 and non zero for region 2 and 4. We solve (3.2) for $i = 1, 2, ...5$, (3.3) for $i = 2, 3, 4$, and (3.4) and (3.5) for $i = 2, 4$.

3.3 Boundary Conditions

As we solve the Helmholtz equation in the same triple layered geometry as in Chapter 2, the boundary conditions used to solve the equation are the same as simplified in Chapter 2. We first simplify the model by applying symmetry boundary condition at AA' as discussed in Chapter 2, and then apply boundary conditions as shown below. At the left most boundary we assume heat losses through convection, which is given by

$$-K_2 \frac{\partial T_2}{\partial x} = h[T_2 - T_A] \quad \text{at} \quad (x = 0, y), \tag{3.6}$$

where K_2 is thermal conductivity of region 2, T_2 temperature in region 2, $T_A = 300K$ is ambient temperature, and h is heat transfer coefficient at the respective boundary. At the axis of symmetry, we have

$$\frac{\partial T_3}{\partial x} = 0 \quad \text{at} \quad (x = l_1 + \frac{l_2}{2}, y). \tag{3.7}$$

At the top and bottom boundary of region 3, we have

$$\frac{\partial T_3}{\partial y} = 0 \quad \text{at} \quad (x, y = 0) \text{ and } (x, y = L). \tag{3.8}$$

We also assume perfect thermal contact between the interfacing boundaries, so we can conveniently maintain C^0 and C^1 continuity. That means

$$\begin{aligned} T_2(l_1) &= T_3(l_1), \\ \frac{\partial T_2(l_1)}{\partial x} &= \frac{\partial T_3(l_1)}{\partial x}, \end{aligned} \tag{3.9}$$

At the inlet in region 2, we have

$$P_{in} = 0.5\ Pa,\ \text{and}\ T_{in} = 300K\ \text{at}\ (x, y = 0). \tag{3.10}$$

Similarly at the outlet in region 2, we have

$$P_{out} = 0\ Pa,\ \text{and}\ \frac{\partial T_2}{\partial y} = 0\ \text{at}\ (x, y = L). \tag{3.11}$$

Finally, no slip boundary conditions are applied at the external boundaries of channel 2 and 4 as given as

$$\vec{u_2} = 0\ \text{at}\ (x = 0, y)\ \text{and}\ (x = l_2, y). \tag{3.12}$$

3.4 Meshing and Convergence Criteria

Meshing and convergence criteria is the same as we discussed in Chapter 2. But in fluid carrying channel, more elements are concentrated at the interfaces between fluid and lossy layer so as to capture the growth of the thermal boundary.

3.5 Computational Results

3.5.1 Thermal Runaway

Since we have hydrodynamically fully developed fluid flow in the y-direction, heat is being extracted by the fluid from the lossy ceramic because of which temperature is no longer uniform in the y-direction causing a non uniform heating. From Figure 3.2, we observe that even with a hydrodynamically fully developed Poiseuille flow, thermal runaway occurs when local maximum temperature reaches a critical value. The difference between the model with and without fluid flow is the convective heat transfer between lossy solid and fluid. Since we assume small volumetric heat capacity and Reynolds number, amount of

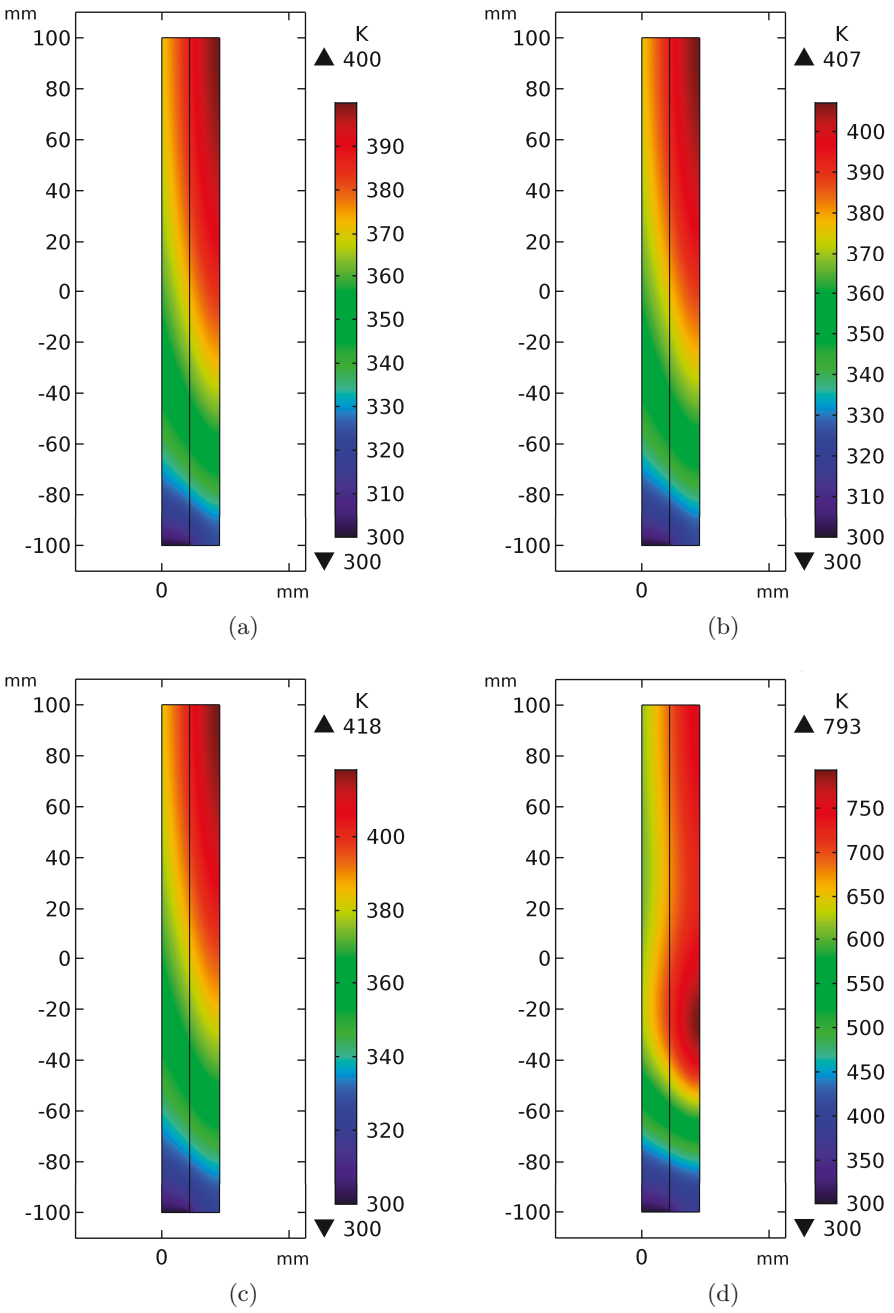

Figure 3.2: Steady-state temperature profiles for different incident powers; (a) P_{av} = 4,200 W/m^2, (b) P_{av} = 4,250 W/m^2, (c) P_{av} = 4,300 W/m^2, and (d) P_{av} = 4,350 W/m^2; initial temperature is 300 K; L= 0.2 m.

heat energy convected away by the fluid is also very small, but the input power at which thermal runaway occur is increased as compared to the critical power for the case with no

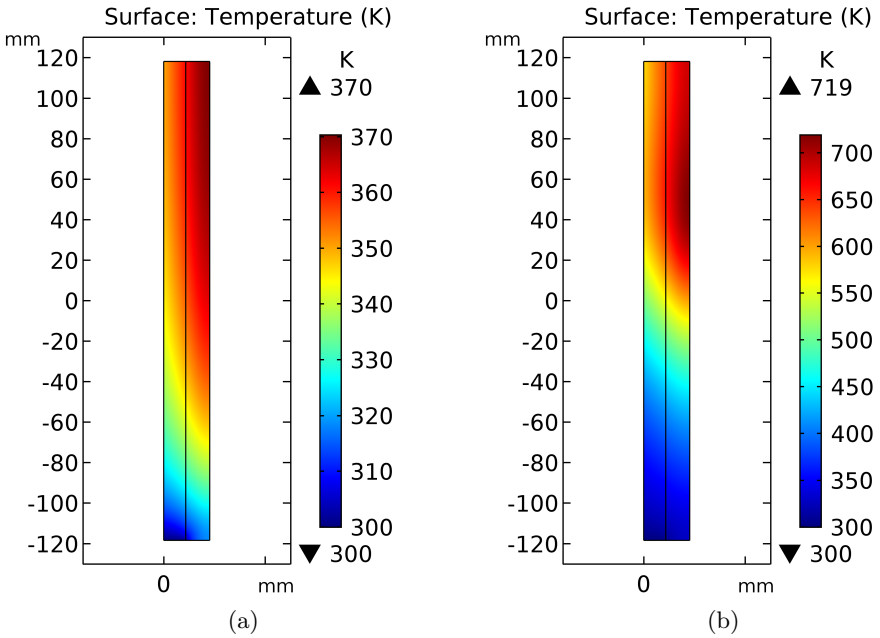

Figure 3.3: Steady state temperature profiles when incident power was 3,750 W/m^2 with initial temperature (a) 300 K and (b) 800 K.

fluid flow (Chapter 2). From Figure 3.2 (d), we see that efficiency of heat exchange between the fluid and the lossy ceramic increases with thermal runaway as compared to non thermal runaway cases.

3.5.2 Multiple Steady States

Figure 3.3 shows two steady state temperature profiles when input power density is kept constant and initial temperature is changed. It is evident that heat energy convected by fluid in Figure 3.3 (b) is much higher. From this result we can expect to see a multi-valued power response curve even for the case with the fluid flow. Whenever multiple steady states are possible, we see different steady state temperatures. From Figure 3.3, we see that for the same input power, we see higher thermal efficiency if initial temperature is different.

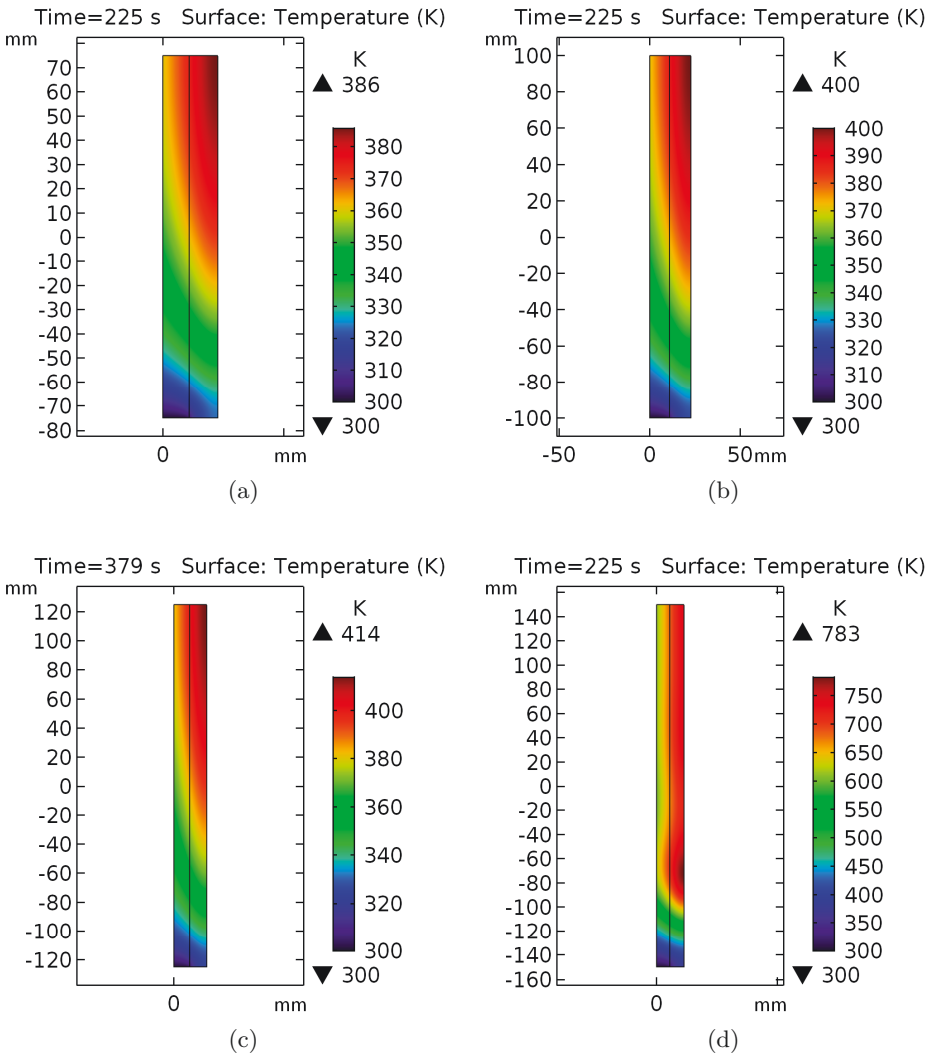

Figure 3.4: Steady-state temperature profiles for different lengths of the channel; (a) L=0.15 m, (b) L=0.20, (c) L=0.25 m, and (d) L=0.30 m; incident power density 4,200 W/m^2.

3.5.3 Effect of Length of the Channel

The steady state temperature patterns in Figure 3.4 show that the maximum temperature T_{max} increases as the length of the channel is increased. When T_{max} reaches a critical value, we observe a large increase in temperature due to thermal runaway. This suggests that high thermal efficiency can be obtained by choosing appropriate length of the channel. As steady-state temperature profiles depend on operating conditions, geometry and material

parameters, the presented model can help determine optimum design parameters of high-efficient triple-layered MHEs.

3.6 Summary

We have developed a 2D numerical model which captures the operation of a triple layered MHE. Even though fluid flow is considered, thermal runaway still initiates when maximum temperature reaches a critical value. We showed that efficiency of a MHE increases when thermal runaway is achieved in the lossy layer. The power at which thermal runaway occurs not only depends on the material parameters, but also on the operating conditions such as geometry, inlet temperature and pressure, external heat transfer coefficient. The developed 2D model can help engineers to develop MHE by choosing optimum design parameters so that thermal runaway is achieved.

Chapter 4

Conclusions

Thermal runaway is a nonlinear phenomenon in which overall temperature increases rapidly with a small increase in incident power. Generally, temperatures during thermal runaway are very high and difficult to control. Such high temperatures, practically instantly, may damage the material itself. However, when appropriate resonance conditions are maintained, temperatures reached during thermal runaway can be maintained within controllable range. This fact motivates us to look at thermal runaway phenomenon as a potential opportunity of efficiently harnessing microwave energy.

In this study, we have found that thermal runaway is triggered by maximum temperatures in the system. Global temperatures increase dramatically as soon as the maximum temperature reaches a critical value. This contention holds true even when fluid flow is incorporated to extract heat generated during thermal runaway. As the amount of heat energy, which is being transferred to fluid from the heated ceramic, increases, incident power required to achieve thermal runaway also increases. On the other hand, we have found that, with appropriate length of the layered microwave heat exchanger, thermal runaway can still be achieved, but at a lower power level. Since we considered a fluid with a very small volumetric heat capacity and Reynolds number, heat energy extracted by the fluid through convective heat transfer is also very small, therefore we do not see significant rise in critical power when we introduce fluid flow. However, when volumetric heat capacity and

effective Reynolds number are high, convection heat transfer between the heated ceramic and the fluid would be dominant, and thus in turn would increase input power required to instigate thermal runaway. Clearly, there exits a trade off between using fluids with high volumetric capacity and geometry of the layered structure.

The numerical model developed in this work captures the basic operation of a layered microwave heat exchanger. We have discussed how thermal runaway can be achieved by increasing the length of fluid carrying channels. The model can further be extended to find out effects of material properties, geometrical parameters, and external operating condition such as frequency of the microwaves, heat transfer coefficient, etc. The critical power level at which thermal runaway occurs not only depends on the material parameters, but also on operating conditions such as geometry, inlet temperature and pressure, external heat transfer coefficient. The developed 2D model can help engineers to design microwave heat exchangers by choosing optimum design parameters so that thermal runaway could be achieved.

We have shown that the efficiency of a MHE increases as thermal runaway is instigated in the lossy layer. When designing an efficient triple layered MHE with actual coolant such as water, we might expect to see a very high critical power, as the volumetric heat capacity of the water is very high. In that case we might need a very long fluid channel. Another important parameter affecting the heat transfer between the heated ceramic and the fluid is the inlet temperature of the fluid. As we increase the inlet temperature of the fluid, amount of heat transferred to the fluid would decrease. We also show that when external heat transfer coefficient increases i.e. convective heat losses to the surrounding increases, critical temperature remains the same but critical power increases proportionally.

Bibliography

[1] A. P. Fraas, *Heat Exchanger Design.* John Wiley & Sons, 1989.

[2] T. L. Bergman, F. P. Incropera, D. P. DeWitt, and A. S. Lavine, *Fundamentals of Heat and Mass Transfer.* John Wiley & Sons, 2011.

[3] W. M. Kays, *Convective Heat and Mass Transfer.* McGraw-Hill, 2012.

[4] C. Metaxas, A, , and R. J. Meredith, *Industrial Microwave Heating.* Peter Peregrinus Ltd., 1983.

[5] M. Willert-Porada, *Advances in Microwave and Radio Frequency Processing.* Springer Verlag, 2006.

[6] J. M. Hill and M. J. Jennings, "Formulation of model equations for heating by microwave radiation," *Applied Mathematical Modelling*, vol. 17, no. 7, pp. 369–379, 1993.

[7] A. Jamar, Z. Majid, W. Azmi, M. Norhafana, and A. Razak, "A review of water heating system for solar energy applications," *Int. Commun. in Heat and Mass Transfer*, vol. 76, pp. 178–187, 2016.

[8] B. Jawdat, B. Hoff, M. Hilario, A. Baros, P. Pelletier, T. Sabo, and F. Dynys, "Composite ceramics for power beaming," in *2017 IEEE Wireless Power Transfer Conference (WPTC), 978-1-5090-4595-3/17*, pp. 1–4.

[9] K. L. Parkin, L. D. DiDomenico, and F. E. Culick, "The microwave thermal thruster concept," in *2nd Intern. Symp. on Beamed Energy Propulsion, 2004*, pp. 418–429.

[10] G. A. Landis, "Beamed energy propulsion for practical interstellar flight," *Journal of the British Interplanetary Society*, vol. 52, pp. 420–423, 1999.

[11] J. C. Coopersmith and E. Davis, "A strategic roadmap for commercializing low-cost beamed energy propulsion launch systems," in *AIAA SPACE 2016*, p. 5555.

[12] J. M. Gaone, B. S. Tilley, and V. V. Yakovlev, "Permittivity-based control of thermal runaway in a triple-layer laminate," in *IEEE MTT-S Intern. Microwave Symp. Dig. (Honolulu, HI, June 2017)*, pp. 459–462.

[13] D. M. Pozar, *Microwave Engineering*. John Wiley & Sons, 2009.

[14] G. A. Kriegsmann, "Thermal runaway in microwave heated ceramics: A one-dimensional model," *Journal of Applied Physics*, vol. 71, no. 4, pp. 1960–1966, 1992.

[15] B. S. Tilley and G. A. Kriegsmann, "Microwave-enhanced chemical vapor infiltration: a sharp interface model," *Journal of Engineering Mathematics*, vol. 41, no. 1, pp. 33–54, 2001.

[16] G. A. Kriegsmann and B. S. Tilley, "Microwave heating of laminate panels," *Journal of Engineering Mathematics*, vol. 44, no. 2, pp. 173–198, 2002.

[17] J. A. Pelesko and G. A. Kriegsmann, "Microwave heating of ceramic laminates," *Journal of Engineering Mathematics*, vol. 32, no. 1, pp. 1–18, 1997.

[18] J. Clemens and C. Saltiel, "Numerical modeling of materials processing in microwave furnaces," *International Journal of Heat and Mass Transfer*, vol. 39, no. 8, pp. 1665–1675, 1996.

[19] V. V. Yakovlev, S. M. Allan, M. L. Fall, and H. S. Shulman, "Computational study of thermal runaway in microwave processing of zirconia," *Microwave and RF Power Applications,* J. Tao, Ed., Cépaduès Éditions, 2011, pp. 303–306.

[20] P. Ratanadecho, K. Aoki, and M. Akahori, "A numerical and experimental investigation of the modeling of microwave heating for liquid layers using a rectangular wave

guide (effects of natural convection and dielectric properties)," *Applied Mathematical Modelling*, vol. 26, no. 3, pp. 449–472, 2002.

[21] J. Zhu, A. V. Kuznetsov, and K. P. Sandeep, "Numerical simulation of forced convection in a duct subjected to microwave heating," *Heat and Mass transfer*, vol. 43, no. 3, pp. 255–264, 2007.

[22] C. M. Sabliov, D. A. Salvi, and D. Boldor, "High frequency electromagnetism, heat transfer and fluid flow coupling in ANSYS multiphysics," *Journal of Microwave Power and Electromagnetic Energy*, vol. 41, no. 4, pp. 5–17, 2006.

[23] D. A. Salvi, D. Boldor, C. M. Sabliov, and K. A. Rusch, "Numerical and experimental analysis of continuous microwave heating of ballast water as preventive treatment for introduction of invasive species." *Journal of Marine Environmental Engineering*, vol. 9, no. 1, 2007.

[24] D. Salvi, J. Ortego, C. Arauz, C. Sabliov, and D. Boldor, "Experimental study of the effect of dielectric and physical properties on temperature distribution in fluids during continuous flow microwave heating," *Journal of Food Engineering*, vol. 93, no. 2, pp. 149–157, 2009.

[25] D. Salvi, D. Boldor, G. Aita, and C. Sabliov, "COMSOL Multiphysics model for continuous flow microwave heating of liquids," *Journal of Food Engineering*, vol. 104, no. 3, pp. 422–429, 2011.

[26] P. D. Muley and D. Boldor, "Multiphysics numerical modeling of the continuous flow microwave-assisted transesterification process," *Journal of Microwave Power and Electromagnetic Energy*, vol. 46, no. 3, pp. 139–162, 2012.

[27] V. V. Yakovlev, "Commercial EM codes suitable for modeling of microwave heating - a comparative review," in *Scientific Computing in Electrical Engineering*. Springer Verlag, 2001, pp. 87–95.

[28] V. V. Yakovlev, "Examination of contemporary electromagnetic software capable of modeling problems of microwave heating," in *Advances in Microwave and Radio Frequency Processing, M. Willert-Porada, Ed.* Springer Verlag, 2006, pp. 178–190.

[29] D. Salvi, D. Boldor, J. Ortego, G. Aita, and C. Sabliov, "Numerical modeling of continuous flow microwave heating: a critical comparison of COMSOL and ANSYS," *Journal of Microwave Power and Electromagnetic Energy*, vol. 44, no. 4, pp. 187–197, 2010.

[30] S. Demjanenko, K. Nowak, R. Northrup, S. Bogachev, E. M. Kiley, D. Bouvard, S. L. Weekes, and V. V. Yakovlev, "Interpolation algorithms for interfacing FDTD and FEM meshes in multiphysics modeling of microwave sintering," in Proc. 12th Seminar "Computer Modeling in Microwave Engineering and Applications - Advances in Modeling of Microwave Sintering" (Grenoble, France, March 2010), pp. 62–64.

[31] X. Wu, "Experimental and Theoretical Study of Microwave Heating of Thermal Runaway Materials," Ph.D. dissertation, Virginia Polytechnic Institute, 2002.

[32] M. Chandran, V. Bogdan Neculaes, D. Brisco, S. Katz, J. Schoonover, and L. Cretegny, "Experimental and numerical studies of microwave power redistribution during thermal runaway," *Journal of Applied Physics*, vol. 114, no. 20, p. 204904, 2013.

[33] "Solving nonlinear static finite element problems," https://www.comsol.com/blogs/solving-nonlinear-static-finite-element-problems, published online: 11-19-2013.

[34] M. N. Sadiku, *Numerical Techniques in Electromagnetics with MATLAB.* CRC Press, 2011.

Appendix A

Procedure of Development of the COMSOL model

1. Open COMSOL Multiphysics 5.3
2. In the **New** window, click **Model Wizard**.
3. In the **Model Wizard** window, click **2D**
4. In the **Select Physics** tree, select **Fluid Flow-Single Phase Flow-Laminar Flow**
5. Click **Add**.
6. In the **Select Physics** tree, select Δu **Mathematics-Classical PDEs-Helmholtz Equation**.
7. Click **Add**.
8. In the **Select Physics** tree, select **Heat Transfer in Solids**.
9. Click **Add**.
10. In the **Study Selection**, select **Empty Study**.
11. Once in the COMSOL environment save the model by selecting **File-Save as**.

12. Include **Global Parameters** by clicking **Home-Parameters**.

13. Define parameters as shown below Table A.1.

Name	Expression	Value
t3	lambda3/2	0.023654 m
t2	3*lambda2/4	0.010891 m
h2	10*t3	0.23654 m
f0	2.45 [GHz]	2.45E9 Hz
ld0	c_const/f0	0.12236 m
ep3	6.69[1]	6.69
lambda3	ld0/sqrt(ep3)	0.047309 m
lambda2	ld0/sqrt(ep2)	0.014522 m
ep2	71[1]	71
P	9000[W/(m^2)]	9000 W/m²
E0	sqrt(2*377[ohm]*P)	2605 V/m
sigma	0.001 [S/m]	0.001 S/m
k0	omega/c_const	51.348 1/m
k2	k0*sqrt(ep2)	432.67 1/m
k3	k0*sqrt(ep3)	132.81 1/m
omega	2*pi*f0	1.5394E10 1/s
nu	sigma/(ep3*omega*8.854e-12[F/m])	0.0010967
TA	300[K]	300 K
Tinlet	300[K]	300 K
Tinitial	300[K]	300 K

Table A.1: Parameters used in the model

14. Define global **Average operator** that computes average of any quantity in domain 1 and 2. We will use this operator later for defining the **stop condition**.

15. Right click on the **Geometry**, click on **Rectangle**; in **Size and Shape** section, set **Width**=t3/2 and **Height**= h2; in **Position** section, set **x:** t2 and **y:** -h2/2.

16. Right click on the **Geometry**, click on **Rectangle**; in **Size and Shape** section, set **Width**=t2 and **Height**= h2; in **Position** section, set **x:** 0 and **y:** -h2/2.

17. Click **Build All Objects**; geometry should look like Figure A.1.

18. Right click on **Materials**, select blank material, set desired thermal material properties.

19. Right click on **Laminar Flow** physics, include **Inlet** and **Outlet** boundary conditions; set desired inlet and outlet pressure if the flow is pressure driven.

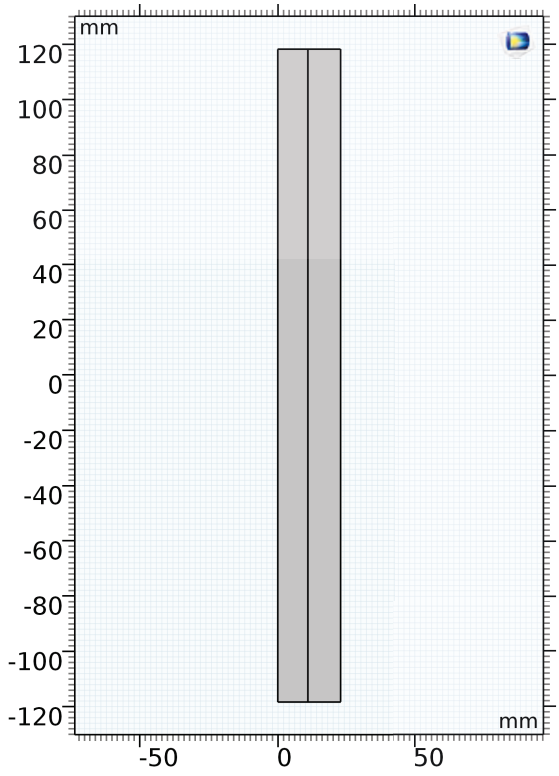

Figure A.1: Geometry of the COMSOL model

20. Right click on **Helmholtz Equation** physics, apply respective boundary conditions discussed in Chapter 2 and Chapter 3 by choosing appropriate **Flux conditions**.

21. Right click on **Heat Transfer** physics, choose domain 1 as **Fluid**.

22. Add volumetric heat source as discussed in Chapter 2.

23. Again by clicking right click, apply respective thermal boundary conditions discussed in Chapter 2 and Chapter 3.

24. Right click on the **Helmholtz Equation** environment, add another **Helmholtz Equation** equation for domain 2. Now we should have two different (for domain 1 and domain 2) Helmholtz equation that can be modified as per material properties of respective domain.

25. In the **Helmholtz Equation** for domain 1, select $c = 1$, $f = 0$, and $a = -(k_2)^2$.

26. Similarly in **Helmholtz Equation** for domain 2, select $c = 1$, $f = 0$, and $a = -(k_3)^2(1 - j * nu * exp(3 * (T - TA)/TA))$ for domain 2. This term should be modified as per the electrical conductivity model.

27. Now add boundary conditions as discussed in Chapter 2 and 3.

28. Add triangular mesh according to the criteria given in Chapter 2 and 3.

29. In order to store value of temperature at previous time step we use **Domain ODEs and DAEs** physics. Set f= u3-nojac(T), da=0, ea=0.

30. Right click on study node, select **study step- time dependent- frequency transient**.

31. Make sure that adaptive time stepping is on, and follows BDF method of order 4.

32. In **Study- solver configuration-** right click on **time dependent solver-**, select **previous solution**, and add variable u3; that we defined in **Domain ODEs and DAEs**.

33. Finally add stop condition by right clicking on **time dependent solver**, and set stopping condition as $abs(comp1.aveop1(comp1.u3) - comp1.aveop1(comp1.T)) <= 1e-6[K]$ and stop if True.

34. Model is now run the simulation and possessor desired results.

Appendix B

Comparison of COMSOL and ANSYS

B.1 Heat Conduction in a Composite Slab

The considered test scenario consists of a composite slab consists of one layer of brick 500 mm thick and two layers of insulation. Inner layer of insulation is 100 mm thick and outer layer is 60 mm. Thermal superconductive of brick, inner, and outer layer are 15 W/mK, 0.12 W/mK, and 0.082 W/mK respectively. The brick side is exposed to gases at 800 ^0C and outer insulation is exposed to ambient air at 30 800 ^0C. Brick side and air side heat transfer coefficients are 300 W/m^2K, and 150 W/m^2K. Find the heat transfer through the slab.

Solution

The above problem is based on 1-D heat transfer, so we can solve the problem by analytical calculations. According to resistance analogy for 1D conduction problem, we can say that medium 1, 2, 3 are in series combination. Therefore, total heat flux through this combination is

$$\dot{q_x} = \frac{T_1 - T_2}{\sum_0^3 R_{th_i}} \tag{B.1}$$

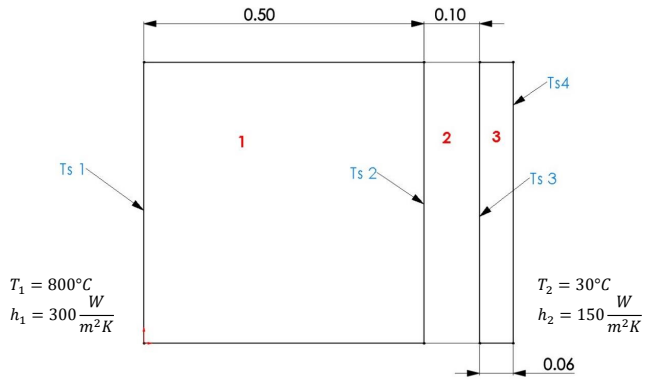

Material	Length (L, m)	Thermal conductivity ($\frac{W}{mK}$)
1	0.5	15
2	0.10	0.12
3	0.06	0.082

Assumptions:
- Steady state
- Constant material properties
- Perfect thermal contact

Ts1	Temperature of the surface which is exposed to hot air
Ts2	Temperature at the contact between material 1 and 2
Ts3	Temperature at the contact between material 2 and 3
Ts4	Temperature of the surface which is exposed to cold air

9

Figure B.1: Geometry of the composit system subjected to 1D heating.

where $\dot{q_x}$ is total heat flow rate through this combination, and R_{th_i} is thermal resistance offered by the medium. Total thermal resistance of the system is

$$R_{th_i} = \left(\frac{1}{h_1 A}\right) + \left(\frac{L_1}{K_1 A}\right) + \left(\frac{L_2}{K_2 A}\right) + \left(\frac{L_3}{K_3 A}\right) + \left(\frac{1}{h_2 A}\right), \tag{B.2}$$

where h_1 is heat transfer coefficient on the left hand side boundary, A is cross sectional area K_1, K_2, and K_3 are thermal conductivity of the respective medium, and h_2 is heat transfer coefficient on the right hand side boundary. Assuming $A = 1\ m^2$, we get $R_{th} = 1.6083\ (K/W)$. Now,

$$\dot{q_x} = \frac{(800 - 30)}{R_{th}} = 478.74\ W/m^2. \tag{B.3}$$

By applying energy balance to the system, we can say that heat flux coming in by convection is equal to flux conducted by the composite wall. Thus we compute $Ts_1 = 798.4041\ ^0C$, $Ts_2 = 782.446\ ^0C$, $Ts_3 = 383.492\ ^0C$, and $Ts_4 = 33.1912\ ^0C$.

Temperature	Analytical results	ANSYS results	COMSOL results
Ts1	798.401 ^0C	798.40 ^0C	798.40 ^0C
Ts2	782.446 ^0C	782.45 ^0C	782.45 ^0C
Ts3	383.492 ^0C	383.45 ^0C	383.49 ^0C
Ts4	33.1912 ^0C	33.192 ^0C	33.192 ^0C

Table B.1: Comparison of results

Conclusion

Table B.1 shows the comparison of numerical and theoretical results. We see results produced by both ANSYS and COMSOL matches with the theoretical results. Both ANSYS Mechanical APDL and COMSOL use Finite Element Method where solution is predicted by assuming linear combinations of shape functions. Since theoretical temperature profile in this 1D conduction problem is a linear function, and as we use linear shape functions in both the packages, FEM can reproduce temperature linear temperature profiles very accurately, as shown in Table B.1.

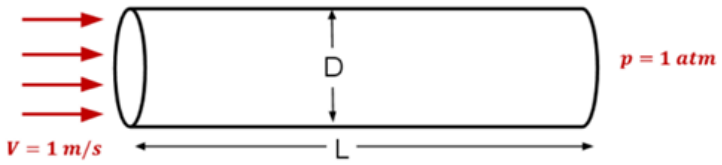

Figure B.2: Geometry considered for modeling laminar fluid flow in a circular pipe.

B.2 Laminar Flow in a Pipe

Consider fluid flowing through a circular pipe of constant radius as illustrated in Figure B.2. The pipe diameter $D = \ 0.2\ m$ and length $L = 3\ m$. Consider the inlet velocity to be constant over the cross-section and equal to 1 m/s. The pressure at the pipe outlet is 1 atm. Take density $\rho = 1\ kg/m^3$ and coefficient of viscosity $\mu = 0.002\ kg/ms$. Determine velocity and pressure profile at the outlet.

Solution

Above problem can be solved by assuming the structure to be axisymmetric i.e., we consider the circumferential component of velocity to be zero ($u_\phi = 0$) in cylindrical coordinate system. Since it is not possible to solve the momentum equations theoretically within developing regions, we assume that the flow is hydrodynamically fully developed (i.e.$u_r = 0$). Mass conservation equations for this geometry are

$$u_r = 0, \tag{B.4}$$

and

$$\frac{du_x}{dx} = 0, \tag{B.5}$$

where u_r is the radial component of the fluid velocity, and u_x is the axial component of the fluid velocity. From momentum equation in radial direction,

$$\frac{\partial P}{\partial r} = 0, \tag{B.6}$$

From (B.5) we conclude say that the axial component of the fluid velocity in fully developed region is changing only in the radial direction, and is constant in the axial direction. From (B.6) we can conclude that the fluid pressure is changing only in the axial direction and not in the radial direction. Finally, the momentum equation in axial direction becomes

$$\mu \left[\frac{1}{r} \frac{d}{dr} \left(r \frac{du}{dr} \right) \right] = \frac{dP}{dx}, \tag{B.7}$$

Left hand side of the (B.7) is a function or r, while right hand side is function of x. Therefore, we can say that

$$\mu \left[\frac{1}{r} \frac{d}{dr} \left(r \frac{du}{dr} \right) \right] = \frac{dP}{dx} = const. \tag{B.8}$$

Integrating above equation twice, we get

$$u(r) = \frac{r^2}{4\mu} \left(\frac{dp}{dx} \right) + C_1 r + C_2 \tag{B.9}$$

Since we have axisymmetric condition at $r = 0$, and no slip conditions at $r = r_0$, we have two boundary conditions along r which are given as

$$\frac{du}{dr} = 0, \text{ at } r = 0, \tag{B.10}$$

and

$$u_r = 0, \text{ at } r = r_0. \tag{B.11}$$

Applying above boundary conditions in (B.9), and solving for C_1 and C_2, we get

$$u(r) = -\frac{r_0^2}{4\mu} \left(\frac{dP}{dx} \right) \left[1 - \frac{r^2}{r_0^2} \right]. \tag{B.12}$$

Since we do not know pressure gradient along the axial direction, we redefine $\frac{dp}{dx}$ in terms of the mean velocity given as

$$u_m = \frac{1}{r^2} \int_0^r u(r) dr, \tag{B.13}$$

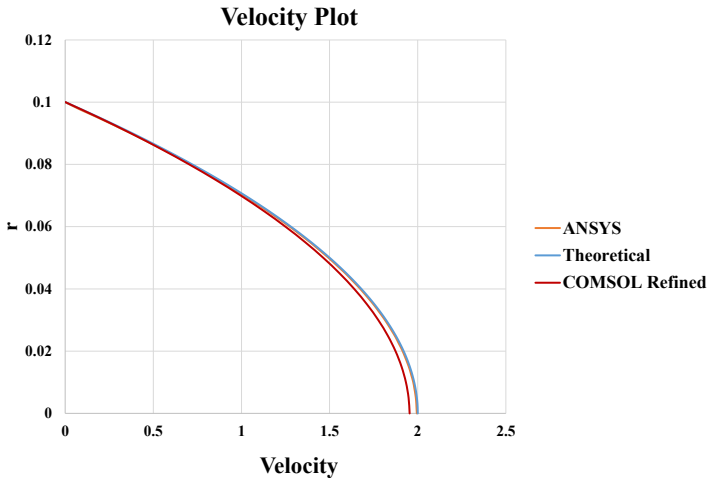

Figure B.3: Comparison of velocity profiles produces by COMSOL and ANSYS Fluent with theoretical solution.

where u_m is the mean velocity. From (B.12) and (B.13), we get

$$u_m = -\frac{r_0^2}{8\mu}\left(\frac{dP}{dx}\right). \tag{B.14}$$

Therefore, final velocity profile for this problem is

$$u(r) = 2u_m\left[1 - \frac{r^2}{r_0^2}\right]. \tag{B.15}$$

Substituting given values, and also solving for pressure profile we get

$$u(r) = 200(0.01 - r^2), \tag{B.16}$$

and

$$P(x) = 1.6(3 - x). \tag{B.17}$$

Comparison with computational results

Figure B.3 shows the comparison of the plot of velocity profile at outlet of the pipe. With the same number of elements, i.e., 4000 elements, COMSOL and ANSYS Fluent showed

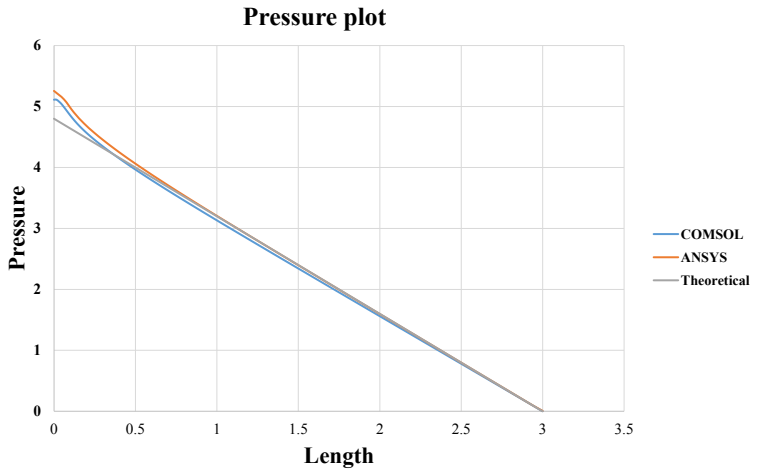

Figure B.4: Comparison of pressure profiles produces by COMSOL and ANSYS Fluent with theoretical solution.

different results. Similarly, Figure B.4 shows the comparison of the axial pressure profiles. Differences seen in the results can be attributed to numerical techniques used by both the software packages. ANSYS Fluent uses Finite Volume Method (FVM), whereas COMSOL uses Finite Element Method (FEM). We can see that COMSOL needs denser mesh to achieve an accuracy as good as ANSYS Fluent.

Appendix C

Comparison of COMSOL and QuickWave

This section of Appendix is focused on electromagnetic module in COMSOL Multiphysics. We comparred results from COMSOL with QuickWave modeling software. COMSOL is a Finite Element Analysis based software whereas QuickWave is a Finite Difference Time Domain based package. Initially patterns of electric field, and electromagnetic power loss were compared to check whether the both packages were producing similar field patterns. In later part, scattering parameters and resonant frequencies were compared. Finally, point to point power loss values (W/m^3) from both COMSOL and QuickWave were compared and root mean squared error was calculated.

Problem statement

For this comparison we consider a 3D model of resonating microwave (MW) cavity as shown in Figure C.1. The geometry consists of a waveguide, a resonating cavity, and a Zirconia dielectric medium. Boundaries of waveguide and cavity were assumed to be Perfect Electrical Conductor (PEC). MW power is fed to the the resonator through a rectangular waveguide, which was excited at the input port. Dimensions of the waveguide were chosen such that dominant mode of electric field is TE_{10}. Since a PEC boundary reflects incident

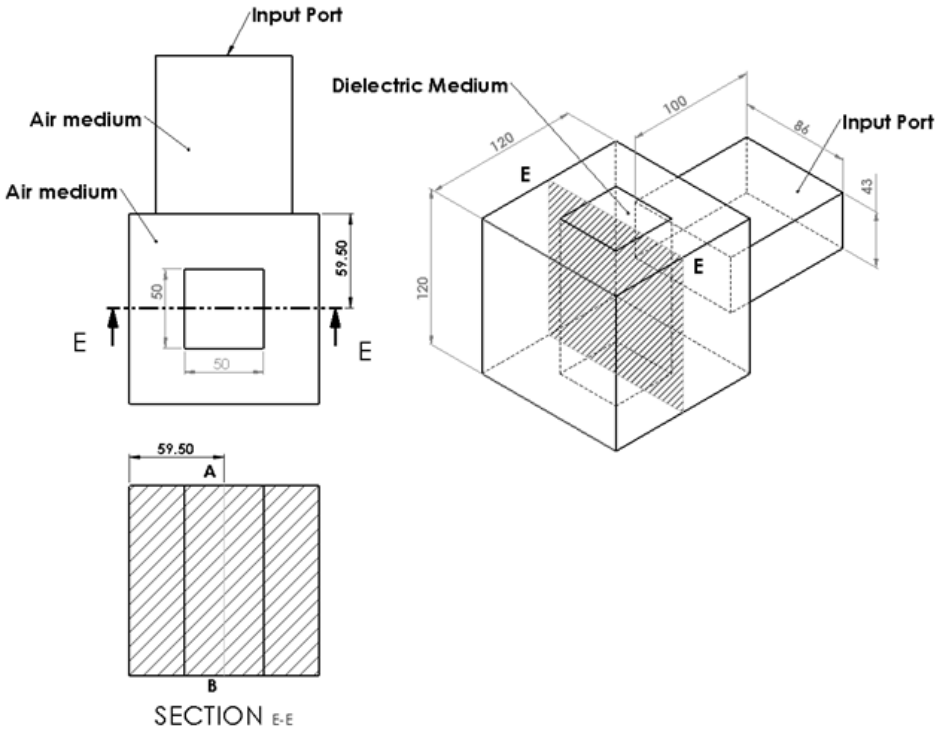

Figure C.1: Geometry of the resonating microwave cavity.

Relative Permittivity ϵ_r	1
Relative Permeability μ_r	1
Electrical conductivity σ	0 S/m

Table C.1: Material properties of free space

Relative Permittivity ϵ_r	6.69
Relative Permeability μ_r	1
Electrical conductivity σ	0.0258 S/m
Specific heat capacity Cp	0.217 J/gC
Density ρ	2.848 g/cm^3
Thermal conductivity K	0.00198 W/cm.C

Table C.2: Material properties of Zirconia

power at the boundary, MW only absorbed in the lossy dielectric medium. Input power is assumed to be 1000 W, and operating frequency of the MW is 2.45 GHz. Material properties used in this simulation are given in Table C.1 and in Table C.2.

	Max Element Size	No of elements
Run 1	24 mm	2,245
Run 2	12 mm	18,598
Run 3	6 mm	159,596
Run 4	4 mm	549,713

Table C.3: Mesh refinements in COMSOL model

	Max Cell Size (in X, Y, Z direction)	No of cells
Run 1	5 mm	28,600
Run 2	4 mm	57,788
Run 3	3 mm	124,394
Run 4	2 mm	419,802
Run 5	1.5 mm	983,016
Run 6	1 mm	3,194,400

Table C.4: Mesh refinement settings used in the QuickWave model

Meshing

As COMSOL is based on Finite Element Analysis, we divide the geometry into Elements, whereas in QuickWave, we divide the geometry in Cells. Discretizing elements for this study were chosen as quadratic and cubic tetrahedron, and cells were of cuboidal shape.

Mesh refinements

We resolve the model with finer and finer meshes, and comparred the change in results between these different meshes. This comparison was done by evaluating the scattering parameter (S_{11}) and the resonant frequency, and power loss in the dielectric medium.

Comparison of S_{11} parameter

As the geometry is a single port microwave circuit, we can only get S_{11} parameter. S_{11} parameter (reflection parameter) is the measure of how much power is leaving the port and getting reflected back to the same port. At the resonant frequency, value of S_{11} parameter is found to be minimum. Even by comparing results at the finest mesh setting (convergent model) in both software we could not get the same values of the resonant frequency and

Run	Resonant Frequency		S_{11}	
	QuickWave	**COMSOL**	**QuickWave**	**COMSOL**
Run 1	2.431	2.456	0.176634	0.253973
Run 2	2.493	2.455	0.185388	0.231285
Run 3	2.444	2.454	0.204850	0.224546
Run 4	2.45	2.454	0.213295	0.222425
Run 5	2.452	NA	0.221429	NA
Run 6	2.453	NA	0.219123	NA

Table C.5: Comparison of S- parameters and resonant frequency given by COMSOL and QuickWave models.

S_{11} parameter.

Summary

Here, we compared results from COMSOL software package with QuickWave software package in modeling resonating MW cavity. Comparison was based on field patterns, S_{11} parameters and the resonant frequency. We find that results produced by both the packages are in a close agreement therefore we conclude that COMSOL is capable of simulating EM phenomenon. Since QuickWave is a FDTD based software, it takes very little time to complete the solution. However, COMSOL model take a long time, however, the use of this software package is imperative in the study undertaken in the present Thesis.